



# Discontinuum Modeling of Solid Deformation Pore-Water Diffusion Coupling

Yifei Cui<sup>1</sup>; Dave Chan<sup>2</sup>; and Alireza Nouri<sup>3</sup>

**Abstract:** This paper presents a numerical scheme for a solid–fluid coupled discrete-element method (DEM) that takes into consideration solid deformation and pore pressure generation and dissipation. Analytical solutions of conventional soil mechanics examples obtained by oedometer testing are used to quantitatively validate the proposed algorithm. The numerical results show good agreement with the analytical solutions. The proposed method advances the current capability of solid–fluid coupled DEM analysis to simulate the mechanical behavior of saturated granular materials. DOI: [10.1061/\(ASCE\)GM.1943-5622.0000903](https://doi.org/10.1061/(ASCE)GM.1943-5622.0000903). © 2017 American Society of Civil Engineers.

**Author keywords:** Discrete-element method; Pore pressure dissipation; Solid deformation pore pressure coupling.

## Introduction

Solid–fluid interactions with pore pressure generation and dissipation are of great interest for applications in geotechnical and petroleum engineering, such as foundation settlement, debris flow, liquefaction, and wellbore drilling. Such problems involve complex interactions between the ground and pore fluid. Solid particles in a porous medium experience changes in the forces exerted by the surrounding fluid as a result of pore pressure changes, and particles also interact with each other and boundary walls on contact. In addition, ground deformation changes the pore volume and thereby changes the pore pressure. However, it is challenging to model solid particle–fluid interactions, including the generation and diffusion of pore-water pressure (PWP).

The discrete-element method (DEM) was first proposed by Cundall and Strack (1979). In the past 30 years, this approach has been developed and applied extensively for solving many geotechnical and petroleum engineering problems. Most DEM applications have been used for dry material (Gong et al. 2012; Chen and Qiu 2012) with no consideration given to water or solid–water interactions. However, the DEM coupled with different computation methods has been developed for fluid dynamics to simulate fluid–particle interactions (Jing et al. 2016).

Tsuji et al. (1993) developed a solid–fluid coupling scheme to simulate fluidized beds. In their study, the fluid phase was discretized into elements larger than the solid particles, and the average pore pressures and fluid velocities were calculated for each element. The fluid force was calculated in each cell and applied to each solid particle. Cook et al. (2002) coupled the DEM with the lattice

Boltzmann (LB) method to simulate the fluid-induced erosive failure of sand particles in a weakly consolidated sandstone and obtained reasonable results. Chan and Tiphavonnukul (2008) developed a coupling method for investigating the hydrotransport of solid particles in pipelines and open channels. They solved the continuity and Navier–Stokes (NS) equations by using a finite-volume scheme with a pressure-correction algorithm. Climent et al. (2014) developed a three-dimensional (3D) DEM–fluid-flow model by coupling the DEM with computational fluid dynamics (CFD). The results agreed with those of the analytical solution provided by Risnes et al. (1982). Takada and Hayakawa (2016) analyzed the drag force that acts on a moving circular disk in a two-dimensional (2D) granular medium by using the DEM. Their simulation focused on the fluid-flow effects on solid particles.

Aside from conventional geotechnical engineering applications, the coupling of DEM and fluid flow has also been applied in other science and engineering fields, such as ocean, material, and chemical engineering. Kafui et al. (2002) developed a fluidized bed model for chemical engineering based on coupling DEM with gas flow. The gas flow was treated as a continuum by solving NS equations. The model was then used to simulate the fluidization of a pseudo-2D particle bed. The results were consistent with the researchers' observations and empirical correlations. Kafui et al. (2011) subsequently proceeded to develop a coupled Lagrangian–Eulerian DEM/CFD parallel code to speed up the calculation process by using multiple computer processors. They simulated the fluidization in a powder bed that comprised 1 million particles and found some of the expected qualitative and quantitative features. A similar coupling analysis was also performed by Guo et al. (2011).

Feng et al. (2007) developed a new method that coupled the LB method with a discrete-element solution for the simulation of particle transport in turbulent fluid flows with a high Reynolds number. The LB method is a microparticle-based explicit time-stepping procedure for obtaining the solution of incompressible fluid flows through use of a fixed regular grid. However, although the core LB operation is effective, the total computational cost can be substantial, because a sufficiently fine lattice is needed, and millions of time steps are required. Latham et al. (2008) used the DEM combined with the finite–DEM (FEM–DEM) to model the granular solid skeleton of randomly packed units and coupled the solid skeleton with a CFD code, which solved wave dynamics through an interface-tracking technique. The coupling work was based on a dual mesh approach. One mesh was used across the whole solution domain in which fluids

<sup>1</sup>Ph.D. Candidate, Dept. of Civil and Environmental Engineering, Univ. of Alberta, Edmonton, AB, Canada T6G 2W2 (corresponding author). E-mail: cui4@ualberta.ca

<sup>2</sup>Professor, Dept. of Civil and Environmental Engineering, Univ. of Alberta, Edmonton, AB, Canada T6G 2W2. E-mail: dave.chan@ualberta.ca

<sup>3</sup>Associate Professor, Dept. of Civil and Environmental Engineering, Univ. of Alberta, Edmonton, AB, Canada T6G 2W2. E-mail: anouri@ualberta.ca

Note. This manuscript was submitted on June 7, 2016; approved on December 16, 2016; published online on March 15, 2017. Discussion period open until August 15, 2017; separate discussions must be submitted for individual papers. This paper is part of the *International Journal of Geomechanics*, © ASCE, ISSN 1532-3641.

equations were solved. A second finite-element mesh was used for solid structures. This approach is computationally less costly than the method used by Feng et al. (2007). Viré et al. (2012) performed modeling of fluid–solid interactions through an adaptive mesh fluid model coupled with a combined finite–discrete-element model. They solved nonhydrostatic NS equations on an unstructured mesh by using the same method that Pain et al. (2001, 2005) used. The method was verified with flow past a falling sphere at small and moderate Reynolds numbers.

When soil or rock is fully saturated with a fluid and the compressibility of water is assumed to be much higher than that of the soil skeleton, isotropic compression or a sudden increase of axial pressure typically causes the reduction of void spaces, which results in an increase in excess PWP. Examples include consolidation in soils with pore-water diffusion and large displacements caused by liquefaction in sands during earthquakes. In either case, the increase in excess PWP causes displacement and deformation of solid particles and void spaces, and the movement of solid particles changes the void spaces occupied by the fluid. This process leads to solid–fluid deformation and causes the fluid to flow. However, none of the DEM methods with fluid flow takes into account the excess generation and dissipation of PWP.

Hakuno and Tarumi (1988) developed a method for modeling liquefaction on the basis of detecting all the pores among particles and connecting them with pipes. The PWP is calculated by assuming a constant volume elasticity for water and water pressure proportional to the pore volume. The fluid flow between each pore space and adjacent pores is calculated on the basis of Darcy's law. This method results in a complicated calculation procedure and requires subsequent manipulation. Nakasa et al. (1999) improved on the method of Hakuno and Tarumi (1988) by implementing square elements that each contain 15 particles. The generation of pore pressure in each cell corresponds to particle movement in neighboring cells and is proportional to the decrease of pore volume. The fluid force applied on the particles depend on the PWP gradient between neighboring cells. Mori et al. (2002) studied the liquefaction of a river dike by applying a 2D discrete-element model. They determined that excess PWP leads to large permanent displacements caused by liquefaction at a microscopic level. In their study, the accumulated excess PWP caused by the combination of shear and effective normal forces was equal to the initial effective normal force. The excess PWP caused by the shear force was related to dissipative energy and stored elastic energy of the model. Bonilla (2004) performed a DEM undrained simulation with fluid coupling by using 2D assemblies of elliptical particles. The pore volume was identified by constructing a polygon that connected the particles around the specified pore space. The volumetric pore changes experienced as a result of particle rearrangements under external forces were then calculated from the volume changes of the polygon. The pore pressure change was then calculated from the pore volume change. The fluid-flow path was constructed using a flow network that joined the centers of the polygons. Pore pressure force was applied to the particles through an integrated method of pore pressure differences on adjacent centers of the polygons. Bonilla (2004) observed temporary liquefaction in their DEM simulations and suggested that the computational efficiency of the method needed improvement. Goodarzi et al. (2015) proposed a numerical scheme for a fluid–particle coupled DEM based on poroelasticity by considering the generation of pore pressure. The fluid was assumed to be a continuum approximated by a Eulerian mesh in a Darcian regime. The pore pressure change was calculated from the volumetric strain. The continuity equation of fluid mesh for a compressible fluid was then solved through the finite-difference

method. On the basis of the pore pressure at the node, hydrodynamic force was applied on each particle in the fluid cell. The method by Goodarzi et al. (2015) was verified on a partially drained case. Catalano and Chareyre (2014) developed a microhydraulic model for granular material that combined the DEM and a pore-scale finite-volume formulation for the flow of an incompressible pore fluid. The model was validated with an oedometer test. However, for the sample in the completely undrained case, the direction of pore pressure–induced force on each particle remained uncertain.

Pore space connectivity and deformation in a porous medium result in uncertainty of the fluid force applied onto individual particles. This paper proposes a new way to incorporate the excess-PWP calculation into a DEM simulation by introducing a new water particle element that has a specific stiffness that enables the calculation of excess pore pressure caused by pore space deformation. This new approach can be used to simulate wet granular deformation with the DEM.

In this paper, PWP is first calculated under the undrained condition. Subsequent dissipation of pore pressure is governed by pore fluid diffusion on the basis of Darcy's law.

## Formulation of a Discrete Model

### DEM

Discrete-element modeling is a numerical method that explicitly models the interaction between particles instead of treating the material as a continuum. The advantages of the DEM are that it provides micromechanical quantities and captures particle-scale interactions that underlie the observed macroscale behavior of soil and rock. However, the micromechanical parameters for DEM analysis cannot be obtained easily from conventional laboratory tests.

DEM analysis involves modeling a granular material with particles that usually have simple geometries, such as spheres in three dimensions or disks in two dimensions. These ideal particles are usually assumed to be rigid, but small overlaps are allowed at the contact points, which are referred to as *soft contacts* (Potyondy and Cundall 2004). At any interparticle contact, a contact stiffness model is used to relate the contact force to the overlapping of the elements. Finite displacements and rotations of discrete bodies, including complete detachment, are allowed among particles.

The formulation of the DEM can be found in the literature. The brief review herein is relevant to the subsequent development of the new water particle element. The calculations performed in the DEM alternate between the application of Newton's second law to the particles and a force-displacement constitutive law applied at the element contacts. Newton's second law is used to determine the translational and rotational motions of each particle that arise from the contact and applied and body forces that act on the particle. The force-displacement law is used to calculate the contact forces that arise from the relative motion at each contact. The force-displacement law explains the relative displacement between two entities at a contact and the contact force that acts on the entities. The DEM calculation flowchart is shown in Fig. 1(a). For both ball–ball and ball–wall contacts, this contact force arises from contact that occurs at a point. The contact force vector  $F_i$  is calculated as shown in Eq. (1)

$$F_i = F_i^n + F_i^s \quad (1)$$

where  $F_i^n$  and  $F_i^s$  = normal and shear force vectors, respectively. The normal and shear forces are calculated by the following formulas:

$$F_i^n = K^n D_i^n \quad (2)$$

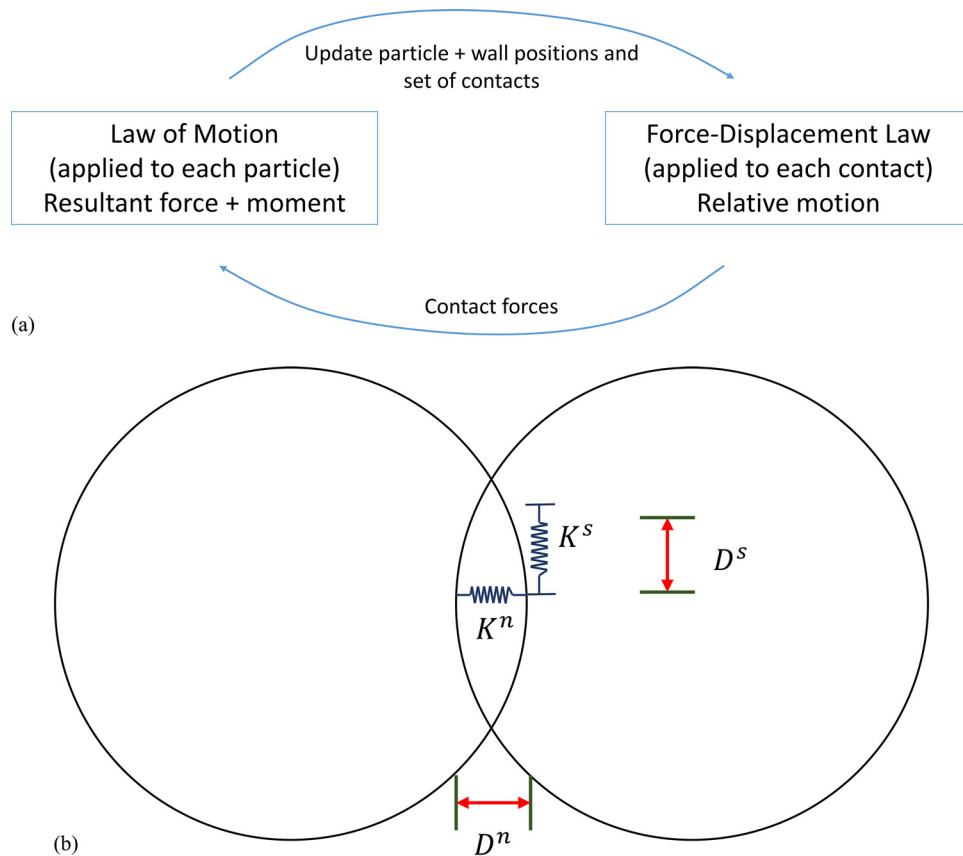


Fig. 1. (a) DEM calculation flowchart; (b) normal and shear contact model

$$F_i^s = K^s D_i^s \quad (3)$$

where  $K^n$  and  $K^s$  = normal and shear stiffnesses at the contact, respectively; and  $D_i^n$  and  $D_i^s$  = contact displacements in the normal and shear directions, respectively. The normal and shear contact model is shown in Fig. 1(b).

The resultant force and moment vectors act on the motion of a single rigid particle, which can be described in terms of translational motion of a point on the particle and the rotational motion of the particle. The equations of motion can be expressed by relating the resultant force to the translational motion and the resultant moment to the rotational motion, which are calculated in Eqs. (4) and (5)

$$F_i = m\ddot{x}_i \text{ (translational motion)} \quad (4)$$

$$M_i = \dot{H}_i \text{ (rotational motion)} \quad (5)$$

where  $F_i$  = resultant force;  $m$  = total mass of the particle;  $\ddot{x}_i$  = acceleration of the specified particle;  $M_i$  = resultant moment acting on the particle; and  $\dot{H}_i$  = angular momentum of the particle.

The incremental velocity is integrated with the displacement of each particle for the current time increment. The locations of all the particles are then updated for the next calculation cycle.

### Coupling of Solid Deformation and Water Diffusion

#### General Formulation

To calculate the PWP generated as a result of discrete-element deformation, a water element that overlaps the solid element is introduced. Because the forces at the contact between the solid elements

represent the effective stress in dry granular material, the introduction of water into the pores reduces the contact forces under the principle of effective stress. To reduce the effective stress caused by the generation of PWP in discrete modeling, the forces at the solid element contact should be reduced. Therefore, the introduced water element increases or decreases the solid contact force as a result of the generation or dissipation of PWP. In this case, the contact forces between the two elements consist of a solid component and a fluid/water component.

In contrast to a solid element, the water element is assumed to have a size and location. The water element also undergoes the same deformation at each contact point, which is similar to solid elements. However, the water element has a stiffness different than that of a solid element. In a DEM analysis of the undrained condition, the total stress is divided into two parts, effective stress and PWP. The effective stress is carried by the solid element, and the PWP is carried by the water element (Fig. 2). The presence of the water element reduces the intersections of particles in the undrained condition in a way similar to that of solid particles (the drained condition).

In the discrete *PFC<sup>3D</sup> 4.0* model, the contact force and particle displacement are computed in  $x$ ,  $y$ , and  $z$  directions (defined by index  $i$  and with the range set as  $i \in \{1,2,3\}$ ) directions. The average stress  $\bar{\sigma}_{ij}$  in a volume  $V$  of material was defined by Nicot et al. (2013) as shown in Eq. (6)

$$\bar{\sigma}_{ij} = \frac{1}{V} \int \sigma_{ij} dV = \frac{1}{V} \sum_{N_p} \bar{\sigma}_{ij}^{(p)} V^{(p)} \quad (6)$$

where  $V$  = total volume of the material;  $\bar{\sigma}_{ij}^{(p)}$  = average stress in a particle ( $p$ );  $V^{(p)}$  = volume of the particle ( $p$ ); and  $N_p$  = number of

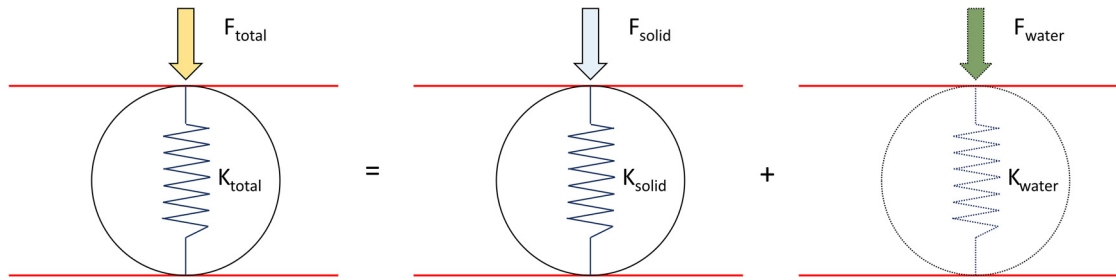


Fig. 2. DEM simulation of effective stress and pore pressure during undrained compression

particles in the control volume. Using the same terms, the average stress in each particle can be written by using Eq. (6) as follows:

$$\bar{\sigma}_{ij}^{(\phi)} = \frac{1}{V^{(\phi)}} \int \sigma_{ij}^{(\phi)} dV^{(\phi)}, \quad \phi = \{p\} \quad (7)$$

The identity  $S_{ij} = \delta_{ik} S_{kj} = x_{i,k} S_{kj} = (x_i S_{kj})_{,k} - x_i S_{kj,k}$  holds for any tensor. Applying this identity to the stress tensor in each particle results in

$$\begin{aligned} \bar{\sigma}_{ij}^{(\phi)} &= \frac{1}{V^{(\phi)}} \int \left\{ [x_i \sigma_{kj}^{(\phi)}]_{,k} - x_i \sigma_{kj,k}^{(\phi)} \right\} dV^{(\phi)} \\ &= \frac{1}{V^{(\phi)}} \{ (I_{ij})_1 - (I_{ij})_2 \} \end{aligned} \quad (8)$$

where the integrals are denoted by  $(I_{ij})_1$  and  $(I_{ij})_2$ . The first integral in Eq. (8) can be rewritten as a surface integral by applying the Gauss divergence theorem such that

$$(I_{ij})_1 = \int [x_i \sigma_{kj}^{(\phi)}]_{,k} dV^{(\phi)} = \int [x_i \sigma_{kj}^{(\phi)}] n_k dS^{(\phi)} = \int x_i t_j^{(\phi)} dS^{(\phi)} \quad (9)$$

where  $S^{(\phi)}$  = boundary surface of the particle;  $n_k$  = unit outward normal force to the boundary surface; and  $t_j^{(\phi)}$  = a traction vector, of which the term  $[x_i \sigma_{kj}^{(\phi)}]$  is assumed to be continuously differentiable. If the moment carried by each parallel bond is neglected and only point forces are applied at the particle contact, the integral in Eq. (9) can be replaced by using the sum of the number of contacts on the surface of the particle  $N_c^{(\phi)}$  as follows:

$$\begin{aligned} (I_{ij})_1 &= \sum_{N_c^{(\phi)}} x_i^{(c)} F_j^{(c,\phi)} \\ x_i^{(c)} &= x_i^{(\phi)} + [x_i^{(c)} - x_i^{(\phi)}] \end{aligned} \quad (10)$$

where  $x_i^{(c)}$  = location of the contact point; and  $x_i^{(\phi)}$  = location of the particle centroid, and  $F_j^{(c,\phi)}$  = force acting on the particle ( $\phi$ ) at contact ( $c$ ). Substituting Eq. (10) into Eq. (9) results in

$$(I_{ij})_1 = \sum_{N_c^{(\phi)}} x_i^{(\phi)} F_j^{(c,\phi)} + \sum_{N_c^{(\phi)}} [x_i^{(c)} - x_i^{(\phi)}] F_j^{(c,\phi)} \quad (11)$$

The second integral in Eq. (8) can be modified by using the equations of motion for the particle ( $\phi$ ), which neglect body forces, under externally applied forces as follows:

$$\sigma_{kj,k} = \rho a_j = \rho \left( \frac{F_j}{m} \right) = \frac{F_j}{V} \quad (12)$$

where  $\rho$  = density;  $a_j$  = acceleration at the centroid; and  $F_j$  = resultant force acting at the centroid. The second integral can be written as the following relation:

$$(I_{ij})_2 = \int x_i \sigma_{kj,k}^{(\phi)} dV^{(\phi)} = \frac{F_j^{(\phi)}}{V^{(\phi)}} \int x_i dV^{(\phi)} = F_j^{(\phi)} x_i^{(\phi)} \quad (13)$$

Substituting Eqs. (13) and (11) into Eq. (8) gives

$$\bar{\sigma}_{ij}^{(\phi)} = \frac{1}{V^{(\phi)}} \sum_{N_c^{(\phi)}} [x_i^{(c)} - x_i^{(\phi)}] F_j^{(c,\phi)} \quad (14)$$

For Eqs. (6)–(14), the particle might not be in static equilibrium, but the body forces should be small compared to the contact forces, and no externally applied force acts on the particle. Substituting Eq. (14) into Eq. (6) results in

$$\bar{\sigma}_{ij} = \frac{1}{V} \sum_{N_p} \bar{\sigma}_{ij}^{(p)} V^{(p)} = \frac{1}{V} \sum_{N_p} \sum_{N_c^{(p)}} [x_i^{(c)} - x_i^{(p)}] F_j^{(c,p)} \quad (15)$$

where  $x_i^{(p)}$  and  $x_i^{(c)}$  = coordinates of the centroid and contact points of a particle, respectively; and  $F_j^{(c,p)}$  = force acting on a particle ( $p$ ) at contact ( $c$ ).  $F_j^{(c,p)}$  includes both contact and parallel-bond normal and shear forces but neglects the moment attributable to the parallel bond. Contact force has both normal and shear components, and the normal component can be calculated from Eq. (16)

$$\begin{aligned} F_j^{(c,p)n} &= K^n D_j^n \\ D_j^n &= D_{\text{total}}^n \frac{x_j^{(p)} - x_j^{(c)}}{\sqrt{\sum_{j=1}^{j=3} [x_j^{(c)} - x_j^{(p)}]^2}} \\ D_{\text{total}}^n &= 2 \left[ R^A - \sqrt{\sum_{j=1}^{j=3} [x_j^{(c)} - x_j^{(p)}]^2} \right] \end{aligned} \quad (16)$$

where  $K^n$  = combined stiffness between the two entities (solid and water) at contact;  $D_j^n$  = particle intersection in the  $x$ ,  $y$ , and  $z$  components, which can be calculated after first finding the total intersection;  $R^A$  = radius of the particle  $A$ ; and  $D_{\text{total}}^n$  = direction normal to the contact plane (Fig. 3).

The PWP (in a water element) can be related to the average stress caused by water particle contact forces, which can be written mathematically as Eq. (17)

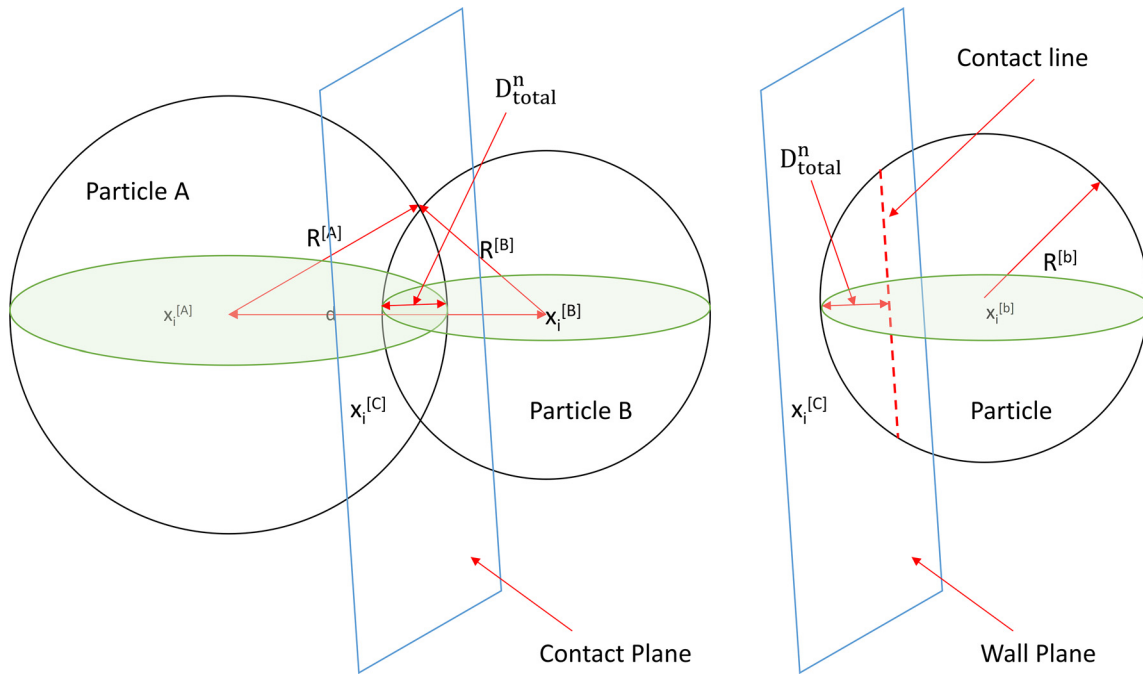


**Fig. 3.** Notations used to describe particle–particle and particle–wall contacts

$$\Delta U = \overline{\sigma_{ii(w)}} = \frac{1}{3} \left( \frac{1}{V_{\text{total}}} \right) \left[ \sum_{i=1}^{i=3} \sum_{N_p} \sum_{N_c^{(p)}} [x_i^{(c)} - x_i^{(p)}] F_{i(w)}^{(c,p)} \right]$$

$$F_{i(w)}^{(c,p)} = K_{w(c)} D_i^n \quad (17)$$

where  $\overline{\sigma_{ii(w)}}$  = stress caused by the fluid element averaged from three principle directions in the sample;  $F_{i(w)}^{(c,p)}$  = contact force exerted by the fluid element;  $K_{w(c)}$  = combined normal stiffness of fluid particles in the linear contact model and calculated from Eq. (18)

$$K_{w(c)} = \frac{K_w K_w}{(K_w + K_w)} = \frac{1}{2} K_w \text{ (for particle – particle contact)}$$

$$K_{w(c)} = \frac{K_w K_{\text{wall}}}{(K_w + K_{\text{wall}})} = \frac{\lambda}{1 + \lambda} K_w \text{ (for particle – wall contact)}$$

(18)

where  $K_w$  = normal stiffness of a single water particle; and  $\alpha$  = ratio between the normal stiffness of the current water particle and contact wall, expressed as  $\lambda = K_{\text{wall}}/K_w$ .

Substituting Eq. (18) into Eq. (17) results in

$$\Delta U = \frac{1}{3V_{\text{total}}} \left[ \sum_{i=1}^{i=3} \sum_{N_p} \sum_{N_c^{(p)}} [x_i^{(c)} - x_i^{(p)}] K_{w(c)} (\eta D_i^n) \right] \quad (19)$$

$$\eta = \begin{cases} \frac{1}{2} & \text{(for particle – particle contact)} \\ \frac{\lambda}{1 + \lambda} & \text{(for particle – wall contact)} \end{cases} \quad (20)$$

Because water particles have 0 shear stiffness, the only unknown is the normal stiffness of the water particle. The pore pressure in an undrained sample is thus averaged in three principle directions; the

water particle stiffness is then calculated by using the averaging method as shown in the following:

$$K_w = (3V_{\text{total}} \Delta U) / \left[ \sum_{i=1}^{i=3} \sum_{N_p} \sum_{N_c^{(p)}} [x_i^{(c)} - x_i^{(p)}] (\eta D_i^n) \right] \quad (21)$$

The compressibility of the soil skeleton  $C_s$  is calculated on the basis of the case of only a solid particle with the DEM. Isotropic stress is applied to the cube sample by using a servocontrol algorithm until the steady state is reached, as shown in the following:

$$C_s = \frac{\Delta V / V_0}{\Delta \sigma}$$

$$\Delta \sigma = \frac{1}{3} (\Delta \sigma_1 + \Delta \sigma_2 + \Delta \sigma_3) \quad (22)$$

where  $V_0$  = initial total volume of the sample;  $\Delta V$  = change in the total volume during stress application;  $\Delta \sigma$  = average total stress increment; and  $\Delta \sigma_1, \Delta \sigma_2, \Delta \sigma_3$  = total stress increase on the sample in the three principle stress directions.

The pore pressure  $B$  parameter is calculated on the basis of fundamental soil mechanics as shown in Eq. (23)

$$B = \frac{1}{1 + n_0 \frac{C_w}{C_s}} \quad (23)$$

where  $C_w$  = compressibility of water and is taken as  $4.6 \times 10^{-10} \text{ m}^2/\text{N}$  in this case; and  $n_0$  = initial porosity of the whole sample.

During the undrained compression stage, stress on the outer boundary is first applied on the sample with solid particles only. The water particle stiffness is then calculated from the pore pressure buildup by porosity changes in Eq. (21). The calculated water particle stiffness is then applied back to the original sample with an outer-boundary total stress of 0 MPa. Then, both the solid and water particles are activated, and they both experience an increase in total

stress that acts on the outer boundary. The same magnitude is also used for the case of only solid particles.

The consolidation process of a soil or porous medium, which is the gradual reduction in the volume of a fully saturated low-permeability soil as the result of drained pore water, continues until the excess PWP is completely dissipated. During this water diffusion process, the excess pore pressure decreases from a maximum value to 0, whereas the effective stress carried by the soil skeleton increases to a value that is equal to the total stress when PWP is 0.

During the water diffusion process, the total stress on the outer-boundary wall is maintained, and the solid stiffness remains unchanged. However, the volume of the total sample decreases as a result of pore water drainage; therefore, the DEM simulations in this study reduce the water particle stiffness by an amount that maintains the expected volume reduction. The total water diffusion process in the DEM simulation is shown in Fig. 4. The pore pressure before the pore pressure dissipation process is calculated from the water particle stiffness in Eq. (17).

### Loose Packing

To calculate the water particle stiffness for various degrees of consolidation or stages of pore water diffusion, several particle-packing configurations are taken into consideration. The calculation of water particle stiffness is important, because it controls the components of the contact force that will be supported primarily by the water element and the remaining part supported by the solid element. By changing the stiffness of the water element, different degrees of consolidation can be simulated by changing the forces supported by the water.

First, the loosest particle-packing configuration with a uniform particle size is considered for a one-dimensional (1D) consolidation analysis (Fig. 5). The force between the particles is transmitted only in the vertical direction along the  $z$ -axis. No Poisson effect occurs in this case, because no lateral deformation is caused by vertical forces. This is characteristic of rigid particles with deformable contacts. Therefore, during the dissipation process (drained condition), no force acts on the side walls in the  $x$  or  $y$  direction.

During consolidation, the PWP can be converted into particle contact force between two particles calculated from the water particle stiffness and is calculated by using Eq. (24)

$$u_1 = \alpha u_0 \quad (24)$$

$$F_{w1} = \alpha F_{w0} \quad (25)$$

where  $u_0$  and  $u_1$  = pore pressure in the sample before and after dissipation occurs, respectively;  $F_{w0}$  and  $F_{w1}$  = force at the contact between two particles calculated from water particle stiffness before and after pore pressure reduction, respectively; and  $\alpha$  = reduction factor that ranges from 0 to 1. The force induced by the water element stiffness is calculated with Eq. (26)

$$\begin{aligned} F_{w0} &= \Delta_0 K_{w0(c)} \\ F_{w1} &= \Delta_1 K_{w1(c)} \\ K_{w0(c)} &= \frac{1}{2} K_{w0} \\ K_{w1(c)} &= \frac{1}{2} K_{w1} \end{aligned} \quad (26)$$

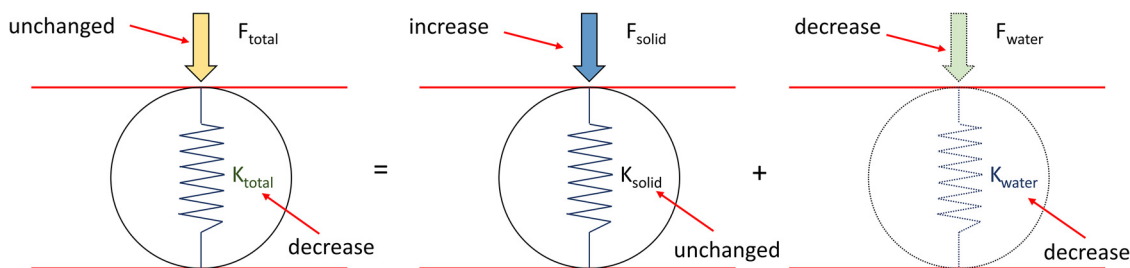


Fig. 4. DEM simulation of effective stress and pore pressure during water diffusion

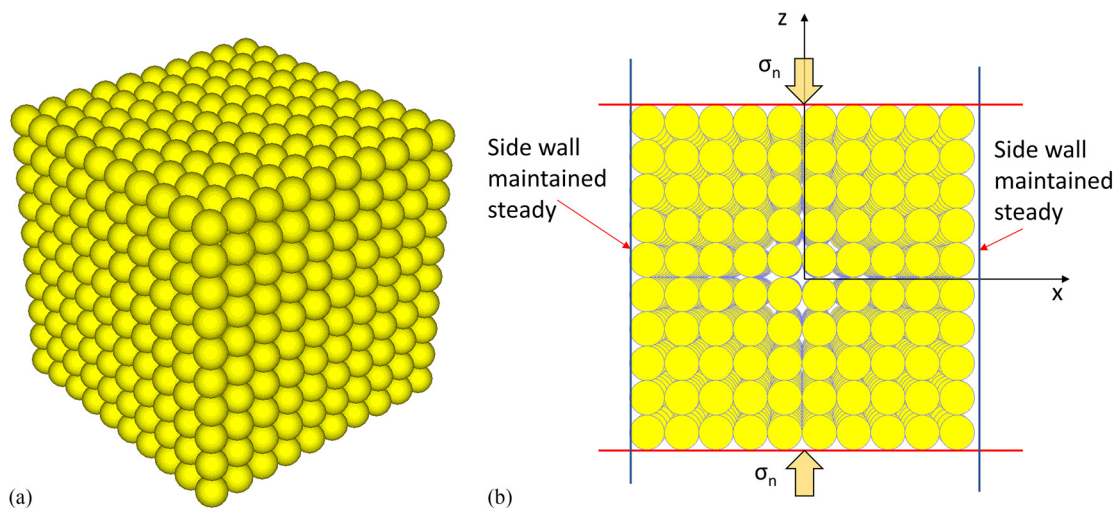


Fig. 5. DEM formulation of loose particle packing: (a) 3D view; (b)  $x$ - $z$  plane view

where  $K_{w0}$  and  $K_{w1}$  = water particle stiffness before and after the pore pressure reduction, respectively;  $\Delta_0$  and  $\Delta_1$  = particle–particle intersection before and after pore pressure reduction, respectively; and  $K_{s0}$  and  $K_{s1}$  = water particle stiffness before and after pore pressure dissipation, respectively. Subscript (c) = combined stiffness at a contact point.

During the pore pressure dissipation process, the total force at a contact point is assumed to be unchanged and calculated with the following equation:

$$F_T = F_{s0} + F_{w0} = F_{s1} + F_{w1} \quad (27)$$

where  $F_{s0}$  and  $F_{s1}$  = force at the contact calculated from solid particle stiffness before and after pore pressure reduction, respectively, as calculated with Eq. (28)

$$\begin{aligned} F_{s0} &= \Delta_0 K_{s(c)} \\ F_{s1} &= \Delta_1 K_{s(c)} \end{aligned} \quad (28)$$

$$K_{s(c)} = \frac{1}{2} K_s \quad (29)$$

where  $K_s$  = solid particle stiffness, which is a constant during the pore pressure dissipation process; and subscript (c) = combined stiffness at a contact point. When Eqs. (26)–(29) are combined with Eq. (25), water particle stiffness after pore pressure reduction is calculated as shown in Eq. (30)

$$K_{w1} = \frac{\alpha K_{w0} \Delta_0 K_s}{2 - \alpha K_{w0} \Delta_0} \quad (30)$$

### Irregular Packing

The random particle packing shown in Fig. 6 shows that the force between the particles is transmitted not only in the vertical direction along the  $z$ -axis for 1D consolidation but also in the horizontal direction along the  $x$ - and  $y$ -axes because of irregular contacts between the particles. Although no deformation is allowed in the  $x$  and  $y$  directions because of the boundary walls, stresses are still

generated on the boundary walls, which means that the linear relationship between a single force induced by a water particle on a contact point and the pore pressure of the whole sample no longer exists. In this case, water particle stiffness can be determined by using an iterative scheme.

During the water pressure dissipation process, a pore pressure dissipation factor,  $\beta$ , is used to calculate the degree of changes in pore pressures, as shown in Eq. (31)

$$u_1 = \beta u_0 \quad (31)$$

where  $u_1$  = pore pressure at the current stage of pore pressure dissipation; and  $u_0$  = initial pore pressure of the whole sample. It is assumed that the changes in pore pressure are uniform through the sample and that contact forces of the water particle change by the same percentage as that of the pore pressure. In other words, the same  $\beta$  value can be used to calculate the current contact force in the water particle, as shown in Eq. (32)

$$\begin{aligned} F_{w1} &= \beta F_{w0} \\ F_{w0} &= \Delta_0 K_{w0} \\ F_{w1} &= \Delta_1 K_{w1} \end{aligned} \quad (32)$$

where  $F_{w0}$  and  $F_{w1}$  = force on a contact point between two particles calculated from water particle stiffness before and after pore pressure reduction, respectively;  $K_{w0}$  and  $K_{w1}$  = water particle stiffness before and after pore pressure reduction, respectively; and  $\Delta_0$  and  $\Delta_1$  = contact intersection between two particles before and after pore pressure reduction, respectively.

The total force  $F_t$  applied to the contact is the same before and after pore pressure dissipation, as shown in the following:

$$F_t = F_s + F_w = K_s \Delta_0 + K_{w0} \Delta_0 = K_s \Delta_1 + K_{w1} \Delta_1 \quad (33)$$

where  $F_s$  and  $F_w$  = contact forces induced by solid and water stiffnesses, respectively; and  $K_s$  = solid particle stiffness, which is maintained as a constant during the pore pressure dissipation process. Assuming that pore pressure reduction is linearly related to changes in the effective stress gives

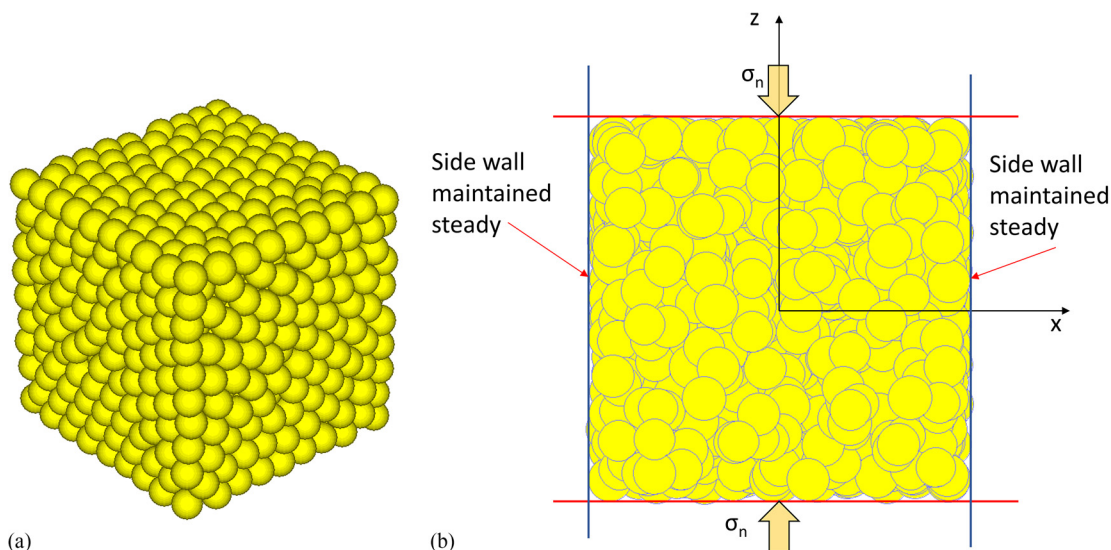
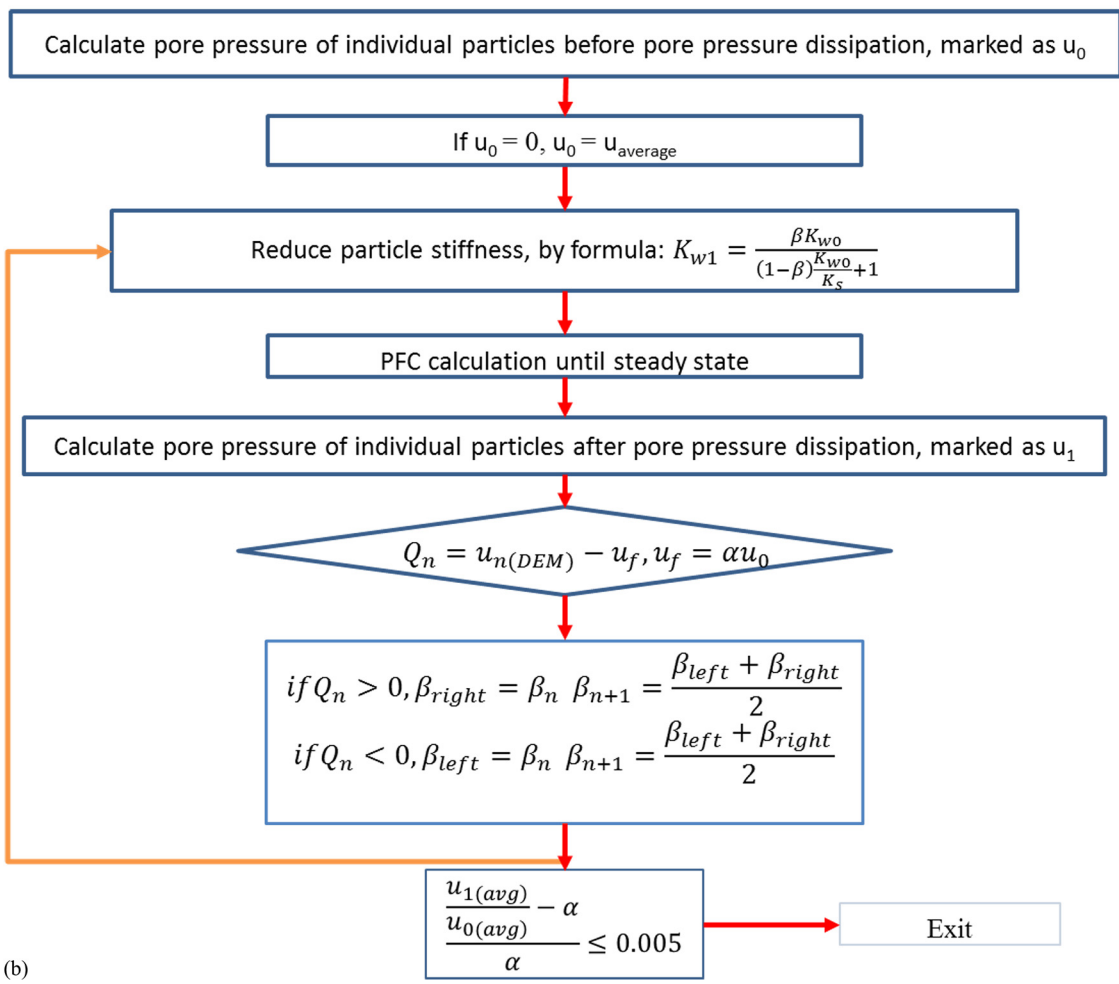
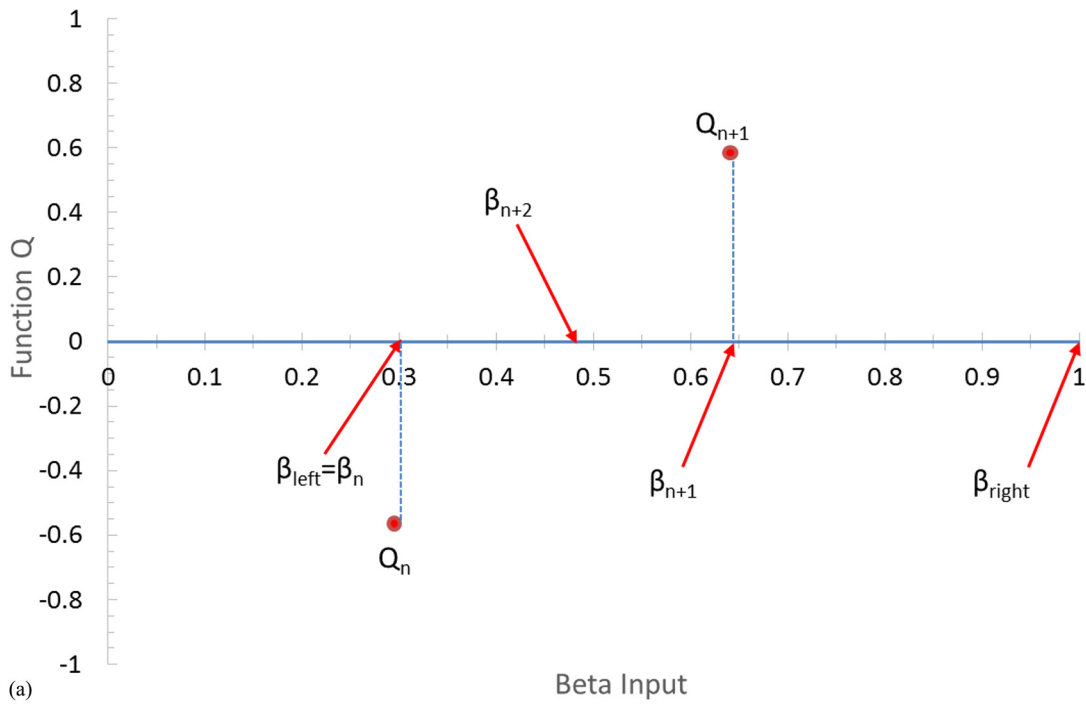
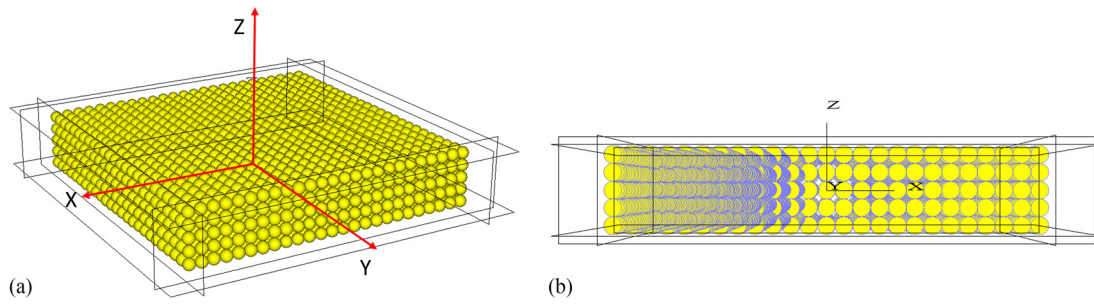


Fig. 6. DEM formulation of irregular particle packing: (a) 3D view; (b) plane view



**Fig. 7.** (a) Bisection method, based on DEM calculations; (b) algorithm for finding corresponding pore pressure dissipation factor



**Fig. 8.** DEM generation of loose particle packing: (a) 3D view; (b) side view (Note: Outer-boundary stress applied only in  $z$  direction)

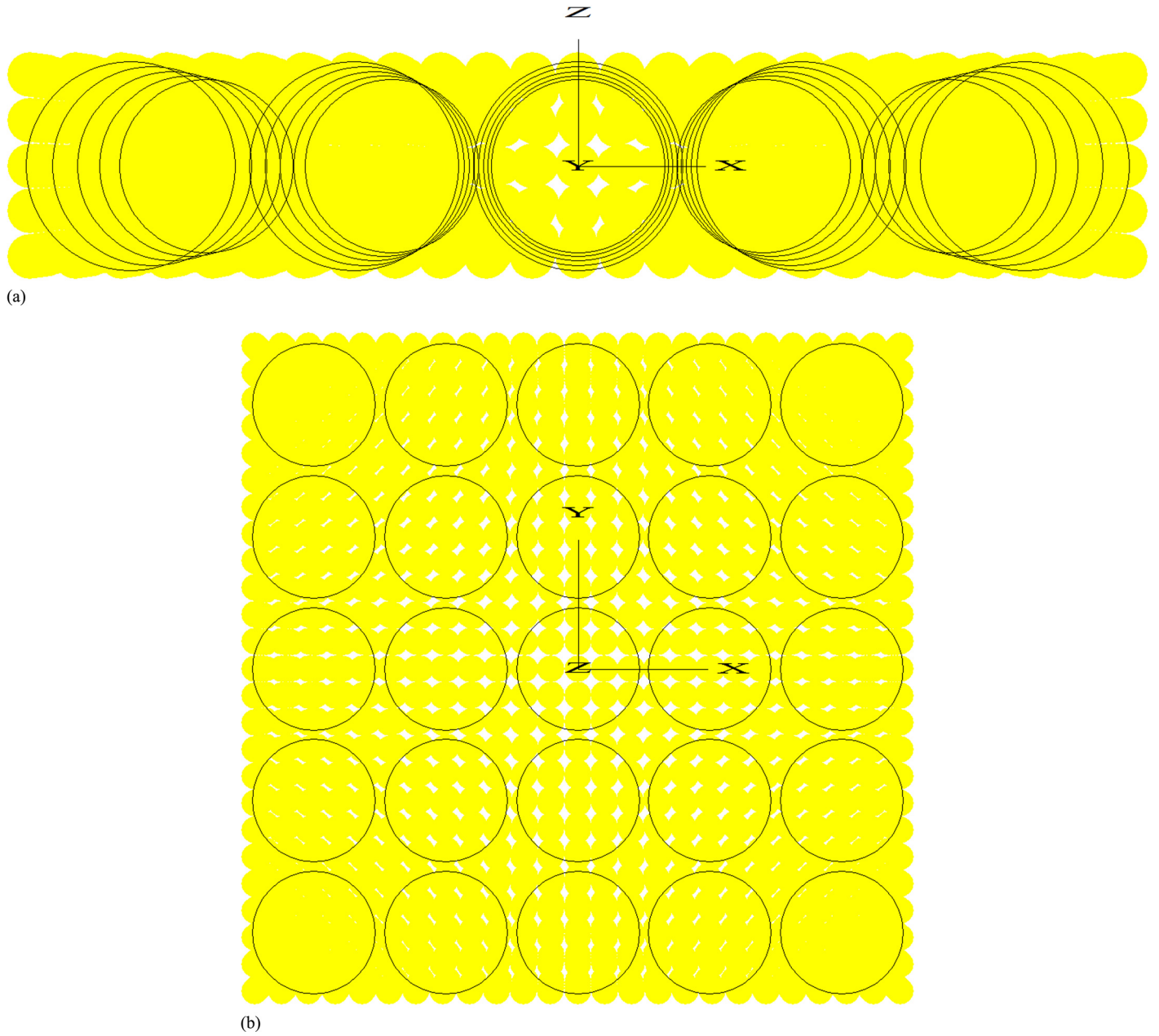


**Fig. 9.** Measurement sphere distribution: (a)  $x$ - $z$  plane view; (b)  $x$ - $y$  plane view

$$K_s \Delta_1 = K_s \Delta_0 \left[ \frac{(1 - \beta) \Delta_0 K_{w0} + K_s \Delta_0}{K_s \Delta_0} \right] \quad (34)$$

By substituting Eq. (34) into Eq. (32), a new water stiffness can be calculated from Eq. (35)

$$K_{w1} = \frac{\beta K_{w0}}{(1 - \beta) \frac{K_{w0}}{K_s} + 1} \quad (35)$$

In DEM calculations, each particle has a unique pore pressure reduction factor,  $\beta_m$ ; therefore, the pore pressure,  $u_m$ , calculations are based on each individual particle,  $m$ , and modified from Eq. (19)

$$u_m = \frac{1 - n_{\text{avg}}}{V_m^{(p)}} \left\{ \sum_{N_c^{(p)}} [x_i^{(c)} - x_i^{(p)}] K_{w(c)} \gamma D_i^n \right\} \quad (36)$$

where  $V_m^{(p)}$  = volume of the individual particle;  $K_{w(c)}$  = combined water stiffness at a contact point between two particles; and  $n_{\text{avg}}$  is the average porosity of the whole sample. Because of the nonlinear relationship between the single force induced by the water particle on a contact point and the pore pressure of the whole sample, the pore pressure dissipation factor,  $\beta$ , cannot be calculated directly from Eq. (32). The final pore pressure dissipation factor,  $\beta$ , is calculated with the bisection method (Chapra 2012), shown as follows:

$$\begin{aligned} Q_n &= u_{n(\text{DEM})} - u_f, u_f = \alpha u_0 \\ \text{if } Q_n > 0, \beta_{\text{right}} &= \beta_n \text{ and } \beta_{n+1} = \frac{\beta_{\text{left}} + \beta_{\text{right}}}{2} \\ \text{if } Q_n < 0, \beta_{\text{left}} &= \beta_n \text{ and } \beta_{n+1} = \frac{\beta_{\text{left}} + \beta_{\text{right}}}{2} \end{aligned} \quad (37)$$

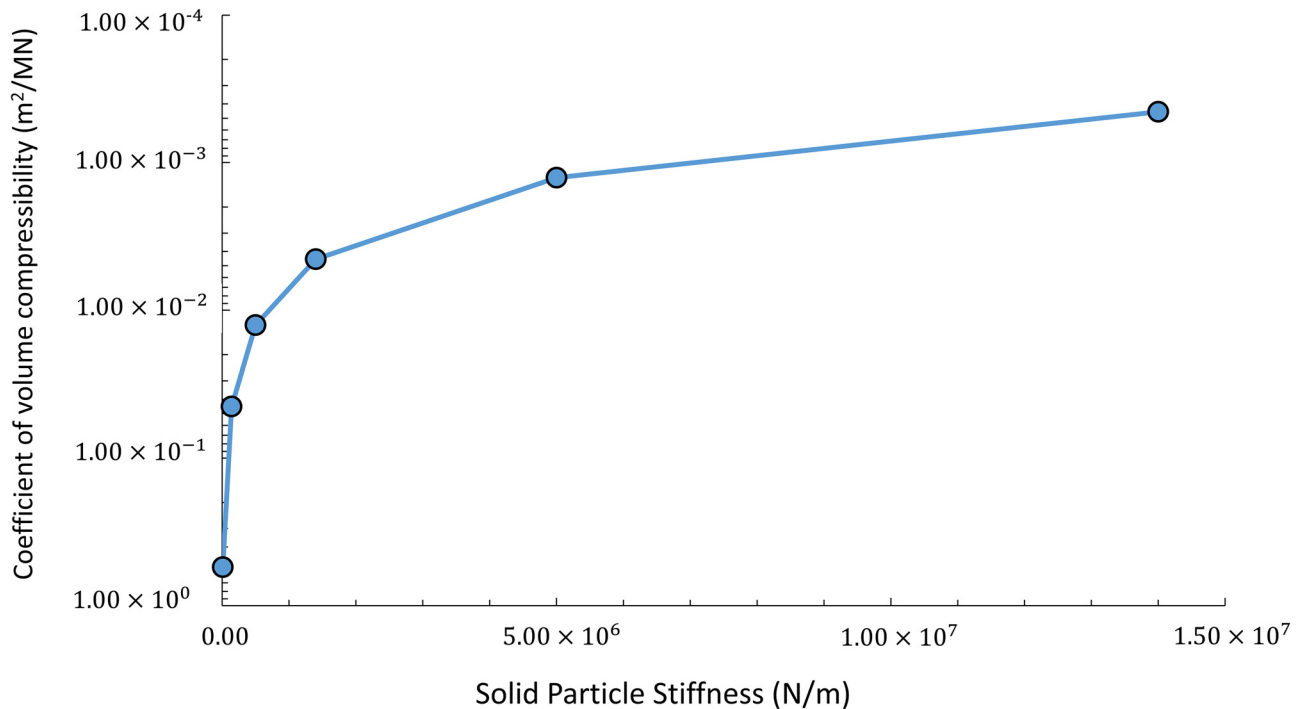


Fig. 10. Variation of volume-compressibility coefficient based on different solid particle stiffnesses

where  $\alpha$  = target pore pressure reduction factor;  $u_{n(\text{DEM})}$  = pore pressure calculated at the end of the current DEM iteration; subscript  $n$  = number of iteration steps; and  $\beta_{\text{left}}$  and  $\beta_{\text{right}}$  are the minimum and maximum boundary values of  $\beta$ , respectively. The first trial values of  $\beta_{\text{left}}$  and  $\beta_{\text{right}}$  are 0 and 1, respectively. The first trial value of  $\beta$  is equal to  $\alpha$ . Then,  $\beta_{n+1}$  is calculated on the basis of boundary values and used in the next iteration. The iterative process continues until the changes in pore pressure are within a specified tolerance from Eq. (38)

$$\frac{u_{n(\text{avg})} - \alpha}{u_{0(\text{avg})}} \leq 0.005 \quad (38)$$

where  $u_{n(\text{avg})}$  = pore pressure calculated by the DEM and averaged from the total number of particles. A graphic depiction of the bisection method used to determine the final pore pressure dissipation factor,  $\beta$ , is shown in Fig. 7(a). The algorithm for the DEM calculations is shown in Fig. 7(b).

## Numerical Modeling of 1D Consolidation of Soil

### Regular Loose Particle Packing Configuration

The DEM model used in the simulation of the 1D consolidation test has a minimum diameter, height, and diameter-to-height ratio of 50 mm, 12 mm, and 2.5, respectively (ASTM 2011). To generate a DEM model that fits this sample size, the length, width, and depth of 75, 75, and 15 mm, bounded by six frictionless rigid walls, are specified. An initial seating load of 10 kPa is applied to all the boundaries, which produces an isotropic stress condition (Fig. 8). Although the model is 3D, the displacement occurs only in the vertical  $z$  direction as a result of the 1D simulation. No deformation is allowed to occur in  $x$  or  $y$  direction, but forces can develop in these

two directions as a result of restraints imposed by the boundary walls.

Measurement spheres are used to calculate the porosity of the sample. The measurement sphere is a built-in tool of *PFC<sup>3D</sup>* that helps the user calculate quantities such as porosity and stress and strain rates through a specific measurement volume. Significant errors in calculating the porosity can occur when the measurement sphere includes only four particles or less. The measurement spheres, therefore, are distributed evenly in the sample and contain at least five particles each. The average porosity of the entire sample is calculated using all the measurement spheres (Fig. 9).

In conventional oedometer consolidation testing, the specimen ring is stiff enough to prevent significant lateral deformation of the specimen throughout testing. Therefore, the stiffness of the boundary wall is set to 5 times the normal particle stiffness. The coefficient of volume compressibility for the soil skeleton can be calculated using the DEM to model 1D compression on solid particles in the dry case as shown in Eq. (39) (Craig 2004)

$$m_v = \frac{1}{1 + e_0} \left( \frac{e_0 - e_1}{\sigma'_1 - \sigma'_0} \right) \quad (39)$$

where  $e_0$  and  $e_1$  = void ratio before and after stress application, respectively; and  $(\sigma'_1 - \sigma'_0)$  = stress increment in the  $z$  direction,

**Table 1.** Particle Microproperties Used in Oedometer Testing of Loose Particles Packing (DEM)

Parameter	Value	Unit
Sample height ( $H$ )	15	mm
Sample length ( $L$ )	75	mm
Sample width ( $W$ )	75	mm
Wall normal stiffness ( $K_{nwall}$ )	$7 \times 10^5$	N/m
Wall stiffness ratio ( $K_{nwall}/K_{swall}$ )	1	—
Particle normal stiffness ( $K_{nball}$ )	$1.4 \times 10^5$	N/m
Particle stiffness ratio ( $K_{nball}/K_{sball}$ )	1	—
Particle radius ( $r$ )	1.5	mm
Particle density ( $\rho$ )	2,650	kg/m <sup>3</sup>
Number of particles	3,125	—
Particle friction coefficient ( $\mu$ )	0.5	—
Initial porosity	0.468	—
Gravity ( $g$ )	9.8	m/s <sup>2</sup>
Compressibility of water ( $C_w$ )	$4.6 \times 10^{-10}$	m <sup>2</sup> /N

which is 0.1 MPa in this case. The variation of the coefficient of volume compressibility based on increasing solid particle stiffness is shown in Fig. 10. The coefficient of volume compressibility increases with increases in solid particle stiffness. The final coefficient of volume compressibility is adjusted to be 0.0447 with particle microproperties as listed in Table 1.

The 1D consolidation process has an initial fully undrained compression stage and a final fully drained stage. The former stage is initiated with an application of vertical stress of 0.1 MPa in the  $z$  direction on the sample with only a solid particle. Water particle stiffness is then calculated from the pore pressure buildup because of the porosity change [Eq. (21)].

The calculated water particle stiffness is then introduced into the DEM calculations, and a boundary stress of 0.01 MPa is reapplied. After the water elements are introduced with finite stiffness, the sample that combined both the solid and water particles supports the stress increment applied on the boundary.

An analytical solution for the consolidation test can be calculated by considering one-half the drained layer (Fig. 11).

The excess pore pressure at any distance  $z$  from the drained layer is calculated by using Eq. (40) (Craig 2004).

$$u_e = \sum_{m=0}^{m=\infty} \frac{2u_i}{M} \left( \sin \frac{Mz}{d} \right) e^{(-M^2 T_v)}; M = \frac{\pi}{2}(2m + 1) \quad (40)$$

where  $u_i$  = initial excess pore pressure;  $d$  = drainage path;  $m$  can be any integer; and  $T_v$  = time factor, calculated as follows:

$$T_v = \frac{C_v t}{d^2}; C_v = \frac{k}{m_v \gamma_w} \quad (41)$$

where  $C_v$  = consolidation coefficient;  $k$  = permeability of clay;  $m_v$  = coefficient of volume compressibility of the soil skeleton; and  $\gamma_w$  = unit weight of water. The basic parameters used in the analytical solution of 1D consolidation are listed in Table 2.

In the analytical solution, the final 1D consolidation settlement of the entire soil layer is calculated on the basis of the change in effective stress, as shown in Eq. (42) (Craig 2004)

$$\Delta H_f = m_v \Delta \sigma' H \quad (42)$$

where  $\Delta \sigma'$  = effective stress change on the soil skeleton (0.1 MPa in this case); and  $H$  = length of drainage layer, which is equal to the depth of the oedometer-tested sample in the  $z$  direction before the dissipation process is initiated.

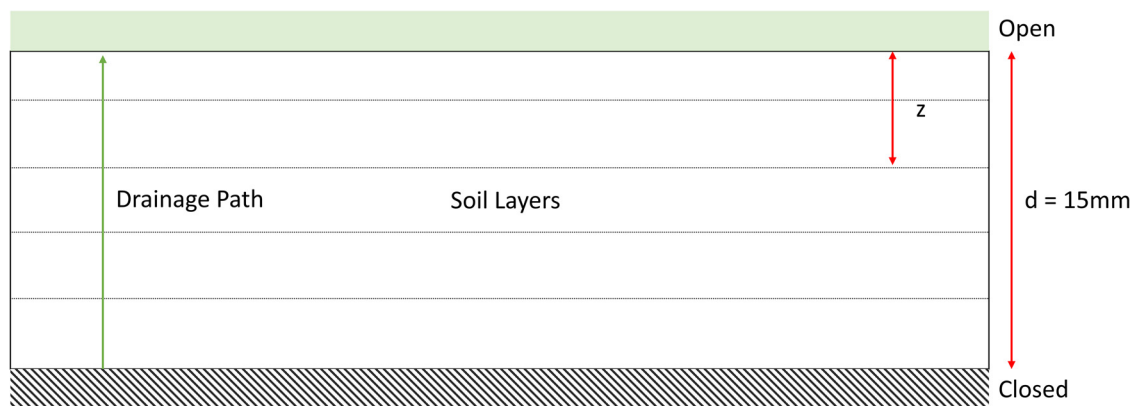


**Fig. 11.** Side view of soil drainage layers for analytical solution

The consolidation settlement of the entire soil layer at any time,  $T_v$ , during the consolidation process is calculated by using the average degree of consolidation,  $U$

$$\Delta H = \Delta H_f(1 - U) \quad (43)$$

$$U = 1 - \sum_{m=0}^{m=\infty} \frac{2}{M^2} \exp(-M^2 T_v) \quad (44)$$

The DEM calculation is divided into five layers for the pore pressure calculation (Fig. 12).

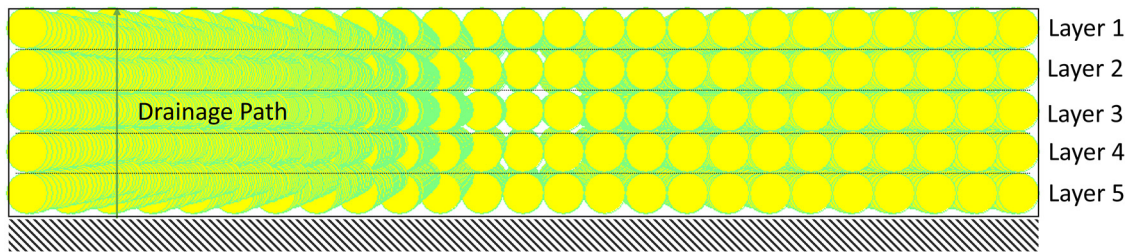
**Table 2.** Basic Soil and Fluid Characteristics in the Analytical 1D Consolidation Test

Parameter	Value	Unit
Permeability ( $k$ )	$1 \times 10^{-10}$	m/s
Coefficient of volume compressibility ( $m_v$ )	0.044742398	$\text{m}^2/\text{MN}$
Unit weight of water ( $\gamma_w$ )	9.81	$\text{kN}/\text{m}^3$
Coefficient of consolidation ( $c_v$ )	$2.2783 \times 10^{-7}$	$\text{m}^2/\text{s}$
Drainage path ( $d$ )	0.015	m
Distance to open drainage ( $z$ )	Case dependent	m
$B$ value	0.99623	—
Initial excess pore pressure ( $u_i$ )	0.09962	MPa

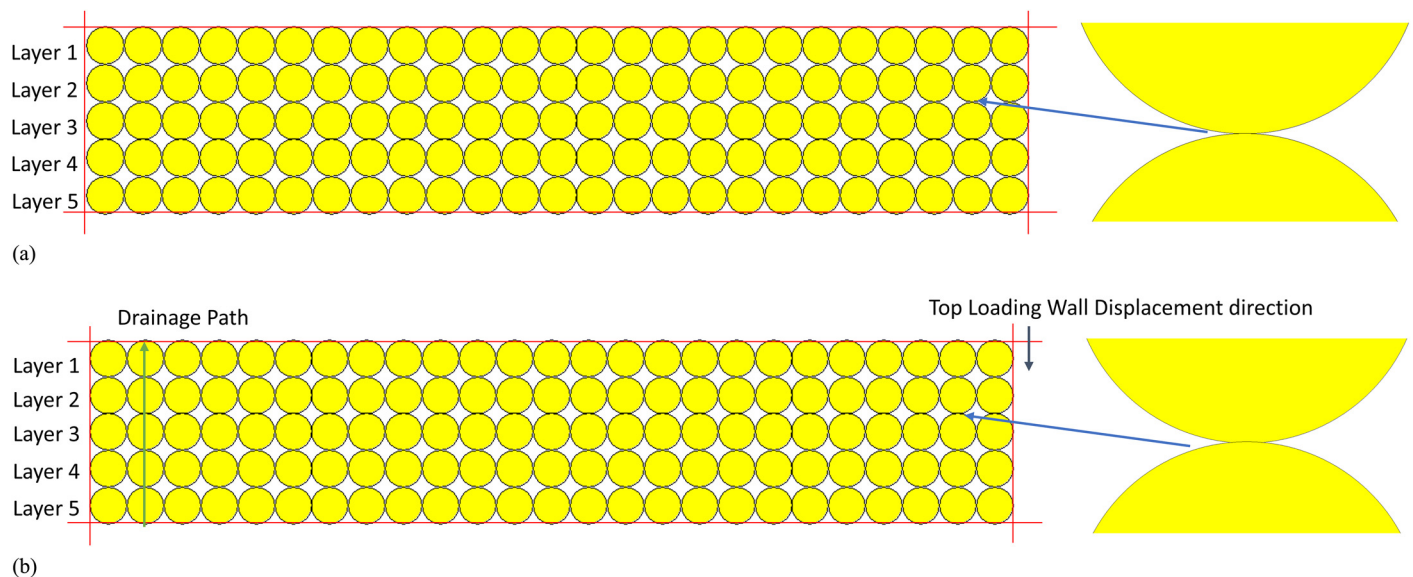
During the drained consolidation test, water particle stiffness is reduced from the maximum value to 0 to correspond to pore pressure decrements at each step [Eq. (30)]. In the analytical solution, the differences in pore pressure at specific times along each layer in the analytical solution [Eq. (40)] result in different stiffness reductions in water particles along each layer. Excess pore pressure of each layer, as determined from the DEM solution, is calculated through Eq. (19). The consolidation settlement of the entire soil layer at any time during the consolidation process is calculated by the difference in displacement between the upper and lower walls in the  $z$  direction.

Fig. 13 compares the particle intersection before (time = 0 s) and after the end (time = 200 s) of pore pressure dissipation. The intersection of particle contact in the  $z$  direction between Layers 2 and 3 increases because of the reduction in water particle stiffness, which leads to the reduction in the total volume of the sample; this finding is consistent with laboratory observations as expected from application of conventional soil mechanics.

Figs. 14(a–e) show comparisons between the DEM and analytical solutions of excess pore-pressure decreases in each layer. Fig. 15 shows comparisons between the analytical and DEM solutions of consolidation settlement of the entire soil sample against time increments. The proposed method can calculate with good accuracy PWP dissipation by using water particles.



**Fig. 12.** Side view of soil drainage layers for DEM calculation of loose particle packing



**Fig. 13.** Intersection of particle contacts: (a) before pore pressure dissipation, time = 0 s; (b) at the end of pore pressure dissipation, time = 2,000 s

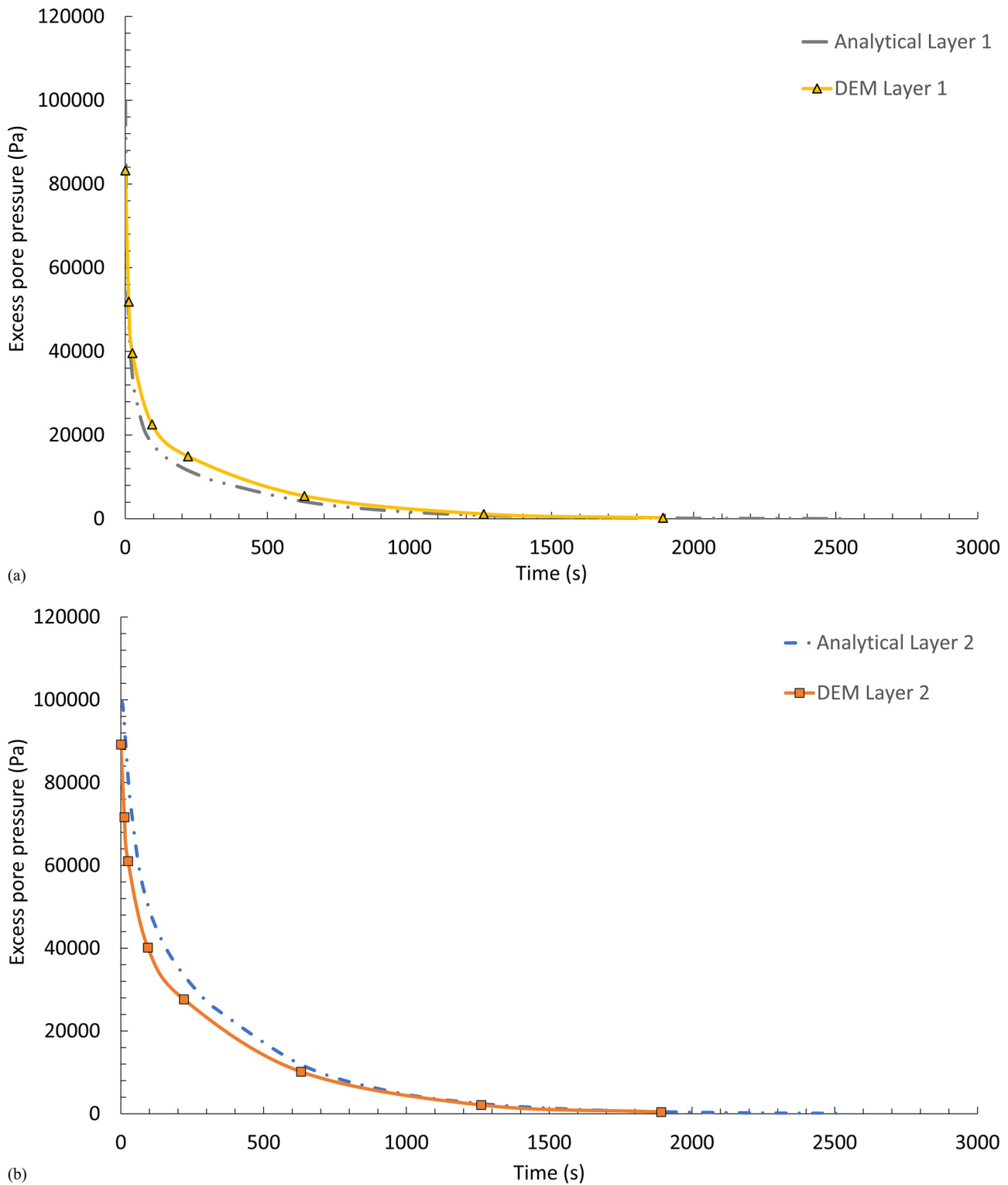


**Fig. 14.** Comparison of excess pore pressure decreases of each layer against time: (a) Layer 1; (b) Layer 2; (c) Layer 3; (d) Layer 4; (e) Layer 5

### ***Irregular Particle Packing Configuration***

A DEM model is generated by using uniformly sized dense irregular particle packing in a rectangular box with a length, width, and depth of 75, 75, and 15 mm, respectively. The elements are bounded by six frictionless rigid walls (Fig. 16). The application of load is 1D, and the boundary walls in the  $x$  and  $y$  directions are fixed by setting the wall velocities to 0. The wall

in the  $z$  direction can move freely on the basis of the servocontrol method.

To calculate sample porosity, a method more precise than insertion of the measurement sphere, as in the loose packing case, is used. Therefore, the total sample volume,  $V_T$ , as illustrated in Fig. 16, is calculated as follows:

$$V_T = \Delta x \cdot \Delta y \cdot \Delta z \quad (45)$$

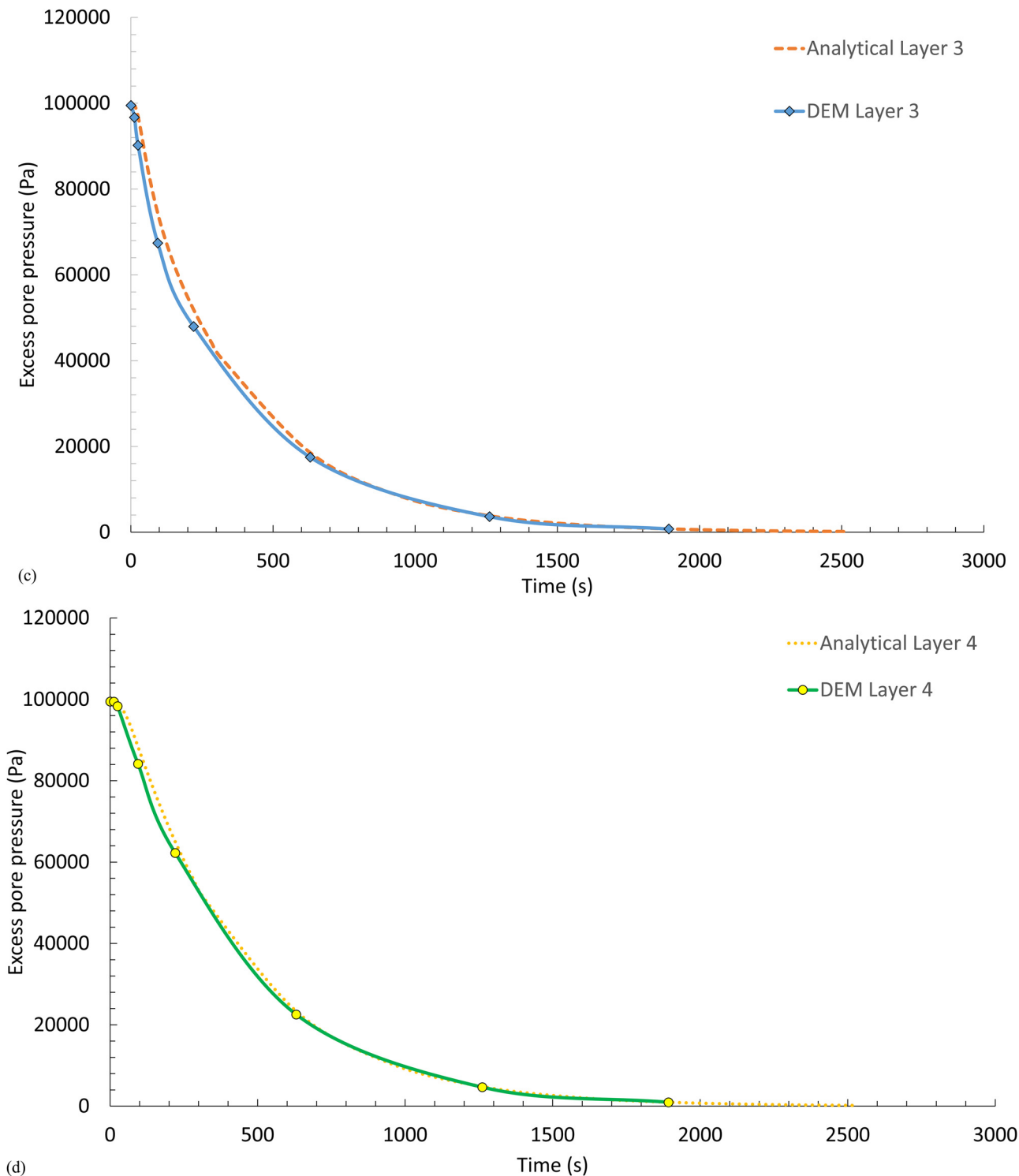


**Fig. 14.** (Continued.)

where  $\Delta x$ ,  $\Delta y$ , and  $\Delta z$  are the perpendicular distances between two walls in the  $x$ ,  $y$ , and  $z$  directions, respectively.

The solid volume,  $V_s$ , is calculated with the following:

$$V_s = V_b^T - V_{b-b}^T - V_{b-w}^T \quad (46)$$

where  $V_b^T$  = total volume of all particles;  $V_{b-b}^T$  = total volume of all particle intersections; and  $V_{b-w}^T$  = total volume of all intersections

between the particles and the wall. The total solid volume of all the particles is calculated from Eq. (47)

$$V_b^T = \sum_{m=0}^{m=N_p} \frac{4}{3} \pi r_m^3 \quad (47)$$

where  $N_p$  = total number of particles in the sample; and  $r_m$  = current particle radius. The volumes for the particle–particle and particle–

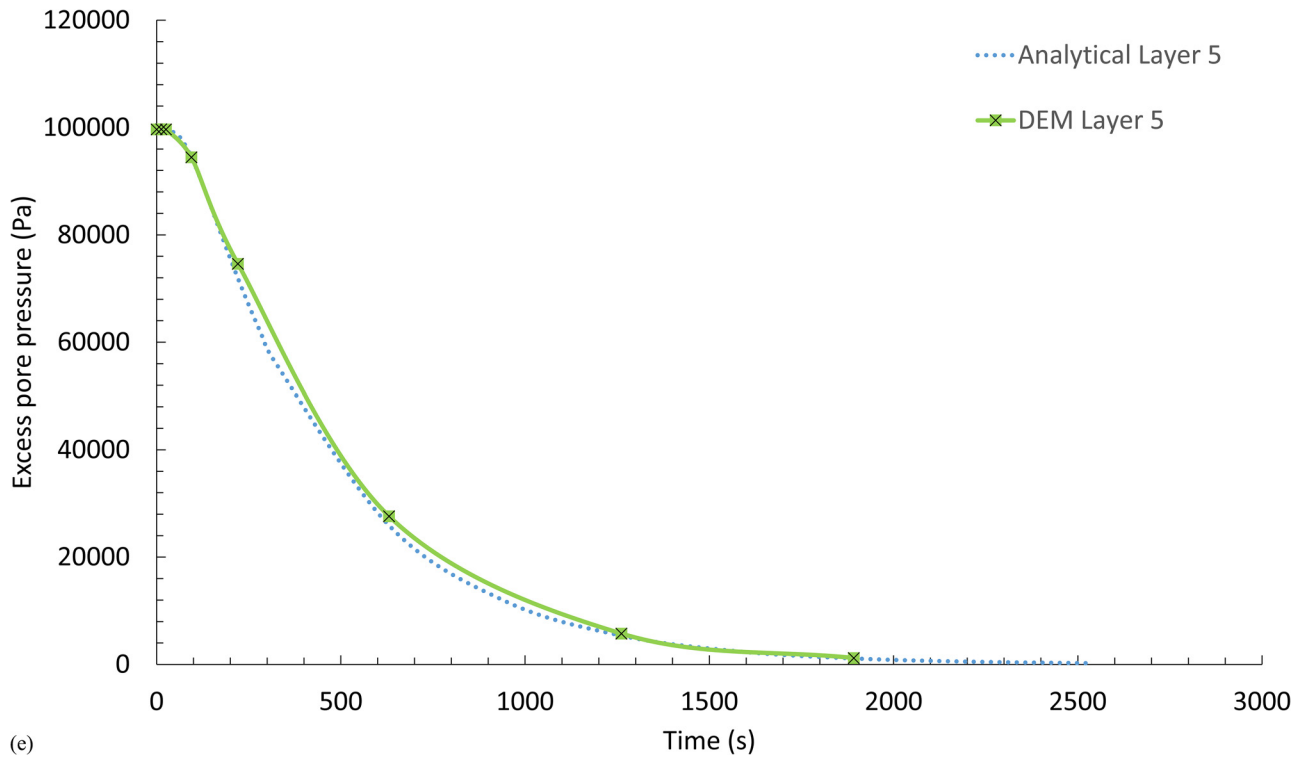


**Fig. 14.** (Continued.)

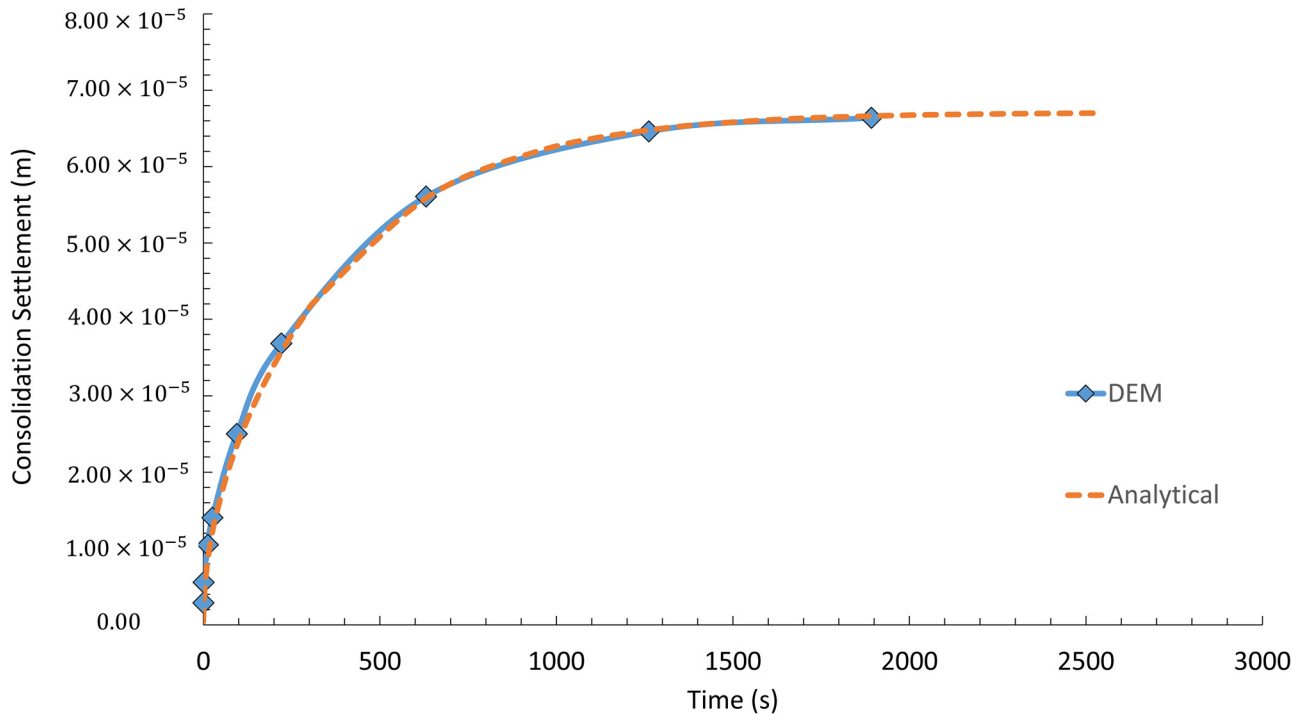


**Fig. 15.** Comparison of consolidation settlements of entire soil sample against time increments between analytical and DEM solutions of loose packing particles

wall intersections are calculated separately and follow the index notation shown in Fig. 3; index  $i$  has a range of  $i \in \{1,2,3\}$  for the  $x$ ,  $y$ , and  $z$  directions. For particle–particle contact, each volume contains

only one-half of the total intersection volume because two particles share one contact. The total intersection volume for particles and particle walls is then calculated by the following equations:

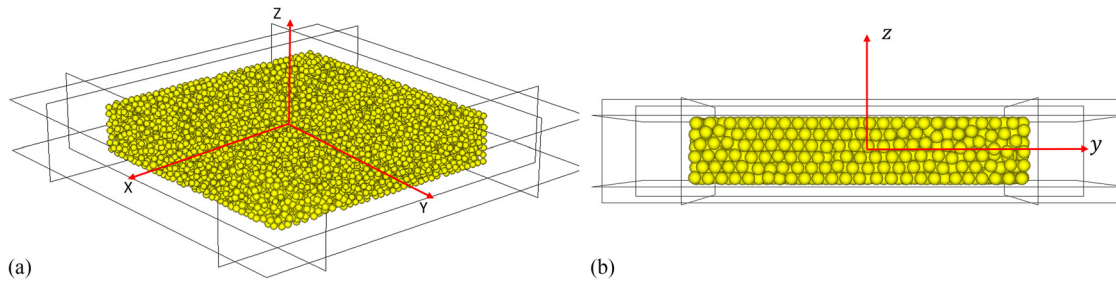


**Fig. 16.** DEM generation of dense particle packing: (a) 3D view; (b) side view (Note: Outer-boundary stress applied only in  $z$  direction)

$$V_{b-b}^T = \sum_{N_p} \sum_{N_c} \frac{1}{2} \left\{ \frac{\pi}{12d} (R^A + R^B - d)^2 [d^2 + 2d(R^A + R^B) - 3(R^A - R^B)^2] \right\} \quad (48)$$

$$d = \sqrt{\sum_{i=1}^{i=3} (x_i^A - x_i^B)^2} \quad (49)$$

$$V_{b-w}^T = \sum_{N_p} \sum_{N_c} \frac{\pi (U_{total}^n)^2}{3} (3r^b - U_{total}^n) \quad (50)$$

$$U_{total}^n = R^b - \sqrt{\sum_{i=1}^{i=3} [x_i^{(c)} - x_i^{(p)}]^2} \quad (51)$$

The true porosity,  $n$ , of the sample is then calculated with Eq. (52)

$$n = \frac{V_v}{V_T} = \frac{V_T - V_s}{V_T} \quad (52)$$

The coefficient of volume compressibility is adjusted following the same procedure as described for the loose packing case. The particle microproperties are listed in Table 3, and the basic parameters used in the analytical 1D consolidation test are listed in Table 4.

The DEM calculation procedure follows the same process and boundary stress (0.1 MPa in the  $z$  direction) as those in the loose packing case. During the dissipation process, the DEM calculation is divided into three layers for pore pressure calculation (Fig. 17). The pore pressure of each layer is first calculated on the basis of the time determined in Eq. (40). The water particle stiffness is then calculated from Eq. (35) and applied on each particle until convergence is reached by using the iteration algorithm (Fig. 7). The iteration for  $\beta$  with the bisection method continues until convergence is satisfied as defined in Eq. (38).

The excess pore pressure of each layer from the DEM solution is calculated from Eq. (17). The consolidation settlement of the entire soil layer at any time during the consolidation process is calculated by calculating the difference in displacement between the upper and lower walls in the  $z$  direction.

Fig. 18 compares the analytical and DEM solutions of excess pore pressure in each layer. The comparison of consolidation settlement of the entire soil sample over time is shown in Fig. 19. The

**Table 3.** Particle Microproperties Applied to Oedometer Testing of Irregular Particle Packing (DEM)

Parameter	Value	Unit
Sample height ( $H$ )	15	mm
Sample length ( $L$ )	75	mm
Sample width ( $W$ )	75	mm
Wall normal stiffness ( $K_{nwall}$ )	$1.5 \times 10^6$	N/m
Wall stiffness ratio ( $K_{nwall}/K_{swall}$ )	1	—
Particle normal stiffness ( $K_{nball}$ )	$3 \times 10^5$	N/m
Particle stiffness ratio ( $K_{nball}/K_{sball}$ )	1	—
Particle radius ( $r$ )	1.5	mm
Particle density ( $\rho$ )	2,650	kg/m <sup>3</sup>
Number of particles	3,879	—
Particle friction coefficient ( $\mu$ )	0.5	—
Initial porosity	0.389	—
Gravity ( $g$ )	9.8	m/s <sup>2</sup>
Compressibility of water ( $C_w$ )	$4.6 \times 10^{-10}$	m <sup>2</sup> /N

**Table 4.** Basic Soil and Fluid Characteristics in Analytical Test of a 1D Consolidation Test

Parameter	Value	Unit
Permeability ( $k$ )	$1 \times 10^{-10}$	m/s
Coefficient of volume compressibility ( $m_v$ )	0.036636473	m <sup>2</sup> /MN
Unit weight of water ( $\gamma_w$ )	9.81	kN/m <sup>3</sup>
Coefficient of consolidation ( $c_v$ )	$2.7824 \times 10^{-7}$	m <sup>2</sup> /s
Drainage path ( $d$ )	0.015	m
Distance to open drainage ( $z$ )	Case dependent	m
$B$ value	0.9952	—
Initial excess pore pressure ( $u_i$ )	0.0995	MPa

analytical and numerical solutions agree well for both pore pressure and displacement changes over time. The accuracy of these simulations reveals the capability of this algorithm to capture solid–fluid interactions.

## Conclusion

In this paper, a new method was presented to model solid–fluid interaction in DEM analysis. The pore pressure buildup caused by solid deformation was captured through use of a water element. During the dissipation process, pore pressure changes were simulated by reducing water particle stiffness as calculated from pore volume reduction. The bisection method was used to calculate the correct water particle stiffness for a specified pore pressure in each

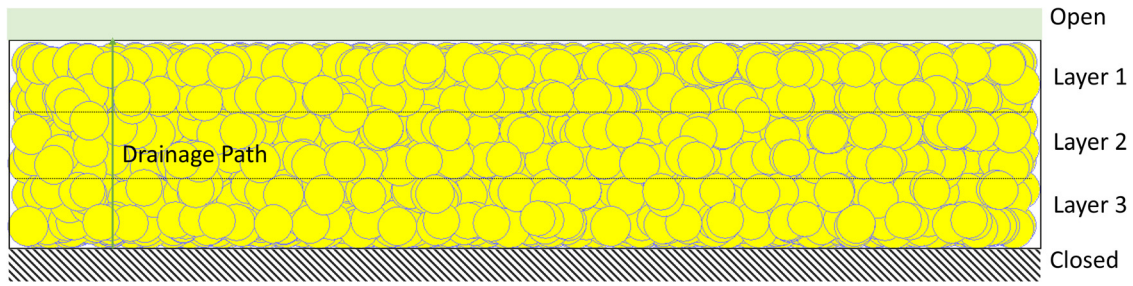


**Fig. 17.** Side views of soil drainage layers for DEM calculation of irregular particle packing

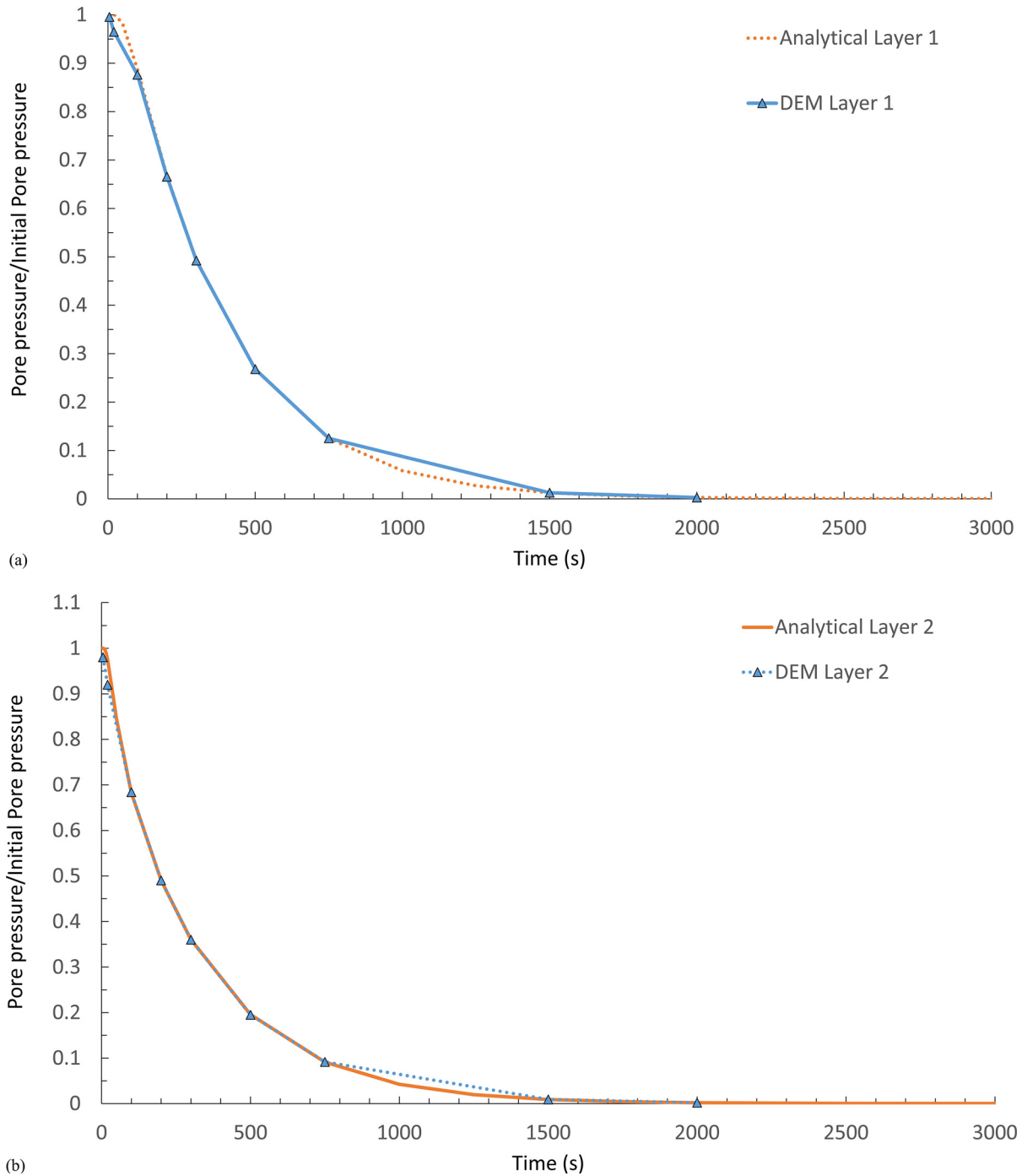


**Fig. 18.** Comparisons of excess pore pressure/initial pore pressure of each layer against time increments between analytical and DEM solutions of irregular particle packing: (a) Layer 1; (b) Layer 2; (c) Layer 3

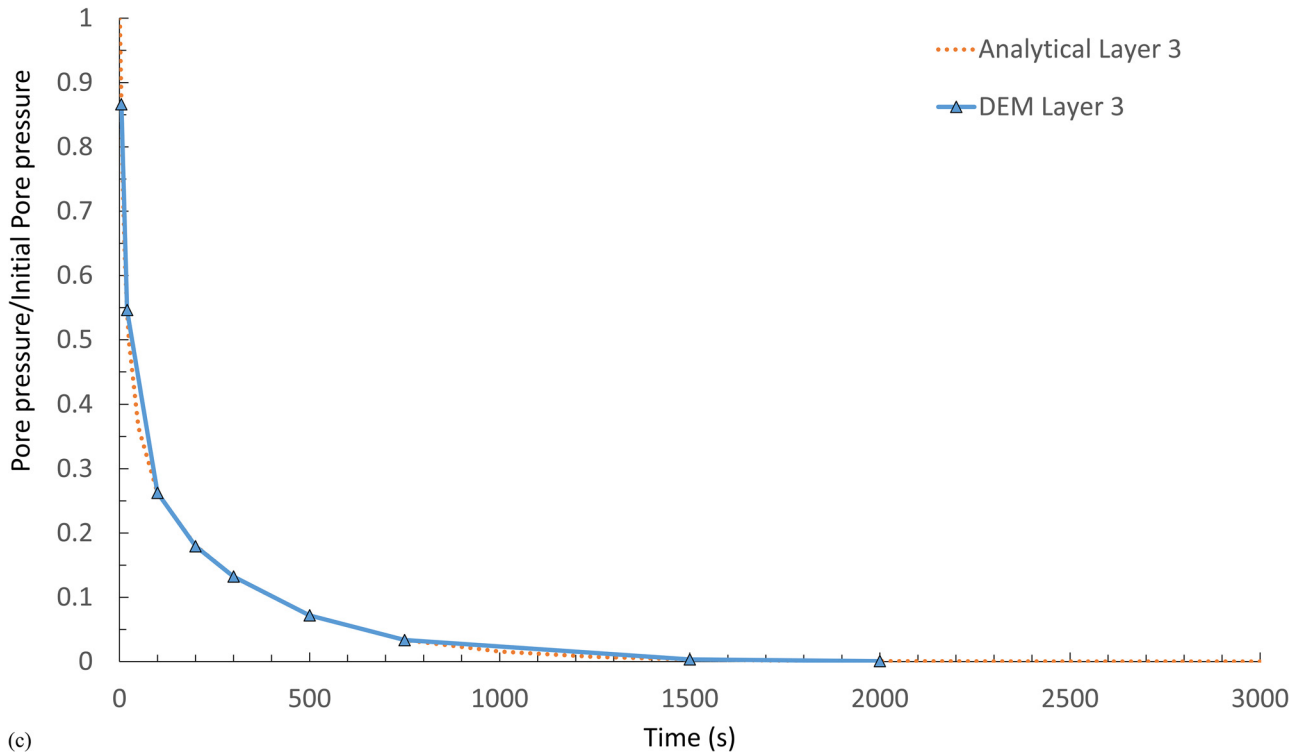


**Fig. 18.** (Continued.)

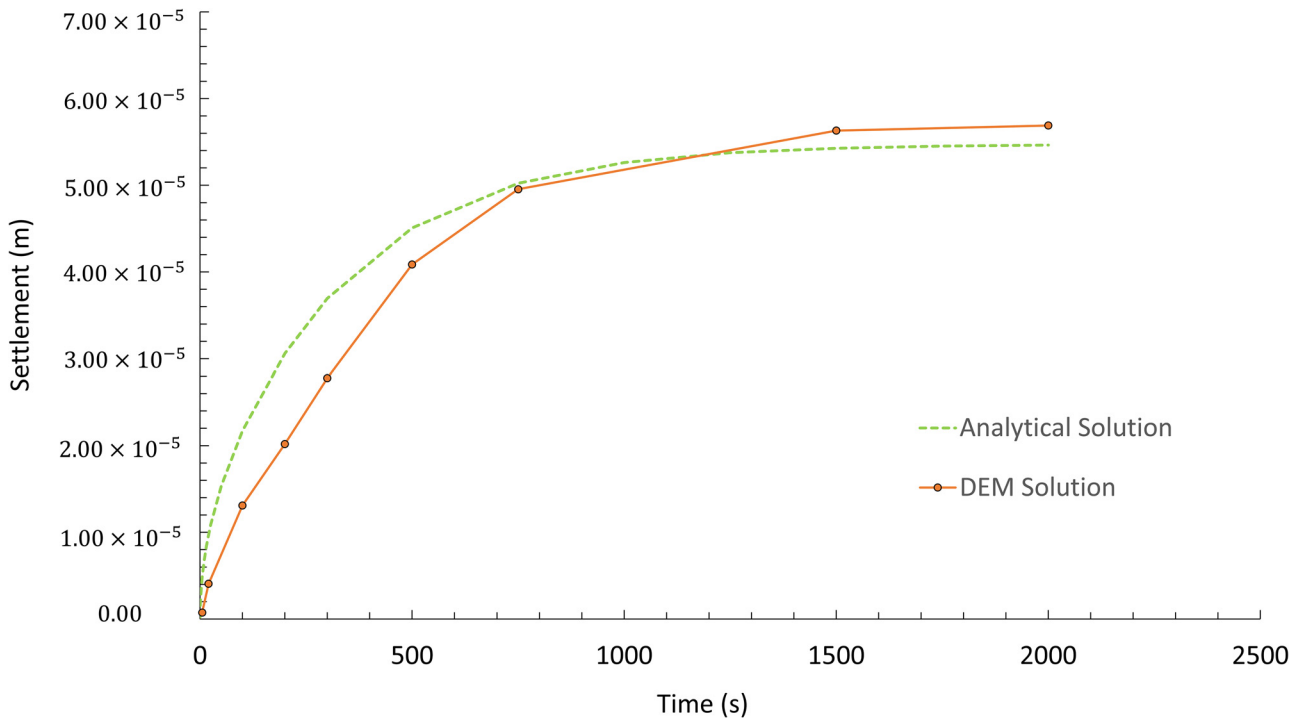


**Fig. 19.** Comparison of consolidation settlement of entire soil sample against time increments between analytical and DEM solutions of irregular particle packing

particle. Analytical solutions based on conventional soil mechanics theory and obtained by oedometer testing were used to validate the proposed algorithm. A comparison between the numerical and

analytical results shows that the DEM model not only replicates the deformation of loosely packed saturated particles but also accurately captures the deformation of densely packed particles.

## Acknowledgments

The authors acknowledge the research funding for this study provided by Canada NSERC through their Discovery Grants Program.

## References

- ASTM. (2011). "Standard test methods for one-dimensional consolidation properties of soils using incremental loading." *D2435/D2435M-11*, West Conshohocken, PA.
- Bonilla, R. R. O. (2004). "Numerical simulations of undrained granular media." Ph.D. thesis, Univ. of Waterloo, Waterloo, On, Canada. (<http://etd.uwaterloo.ca/etd/rroliver2004.pdf>) (Apr. 20, 2016).
- Catalano, E., and Chareyre, B. E. (2014). "Pore-scale modeling of fluid-particles interaction and emerging poromechanical effects." *Int. J. Numer. Anal. Methods Geomech.*, 38(1), 51–71.
- Chan, D., and Tiphavonnukul, S. (2008). "Numerical simulation of granular particles movement in fluid flow." *Int. J. Nonlinear Sci. Numer. Simul.*, 9(3), 229–248.
- Chapra, S. C. (2012). *Applied numerical methods with MATLAB for engineers and scientists*, 3rd Ed., McGraw-Hill, New York.
- Chen, W., and Qiu, T. (2012). "Numerical simulations for large deformation of granular materials using smoothed particle hydrodynamics method." *Int. J. Geomech.*, 10.1061/(ASCE)GM.1943-5622.0000149, 127–135.
- Climent, N., Arroyo, M., O'Sullivan, C., and Gens, A. (2014). "Sand production simulation coupling DEM with CFD." *Eur. J. Environ. Civ. Eng.*, 18(9), 983–1008.
- Cook, B., Noble, D., and Williams, J. (2002). "A coupled DEM-LB model for the simulation of particle-fluid systems." *Proc., 3rd Int. Conf. on Discrete Element Methods*, ASCE, Reston, VA, 161–166.
- Craig, R. F. (2004). *Craig's soil mechanics*, 7th Ed., Taylor & Francis, New York.
- Cundall, P. A., and Strack, O. D. L. (1979). "A discrete numerical model for granular assemblies." *Géotechnique*, 29(1), 47–65.
- Feng, Y. T., Han, K., and Owen, D. R. J. (2007). "Coupled lattice Boltzmann method and discrete element modelling of particle transport in turbulent fluid flow: Computational issues." *Int. J. Numer. Methods Eng.*, 72(9), 1111–1134.
- Gong, G., Thornton, C., and Chan, A. H. C. (2012). "DEM simulations of undrained triaxial behavior of granular material." *J. Eng. Mech.*, 10.1061/(ASCE)EM.1943-7889.0000366, 560–566.
- Goodarzi, M., Kwok, C. Y., and Tham, L. G. (2015). "A continuum-discrete model using Darcy's law: Formulation and verification." *Int. J. Numer. Anal. Methods Geomech.*, 39(3), 327–342.
- Guo, Y., Wu, C.-Y., Kafui, K. D., and Thornton, C. (2011). "3D DEM/CFD analysis of size-induced segregation during die filling." *Powder Technol.*, 206(1–2), 177–188.
- Hakuno, M., and Tarumi, Y. (1988). "Sand liquefaction analysis by granular assembly simulation." *Proc., 9th World Conf. on Earthquake Engineering*, International Association for Earthquake Engineering, Tokyo, 231–236.
- Jing, L., Kwok, C. Y., Leung, Y. F., and Sobral, Y. D. (2016). "Extended CFD-DEM for free-surface flow with multi-size granules." *Int. J. Numer. Anal. Methods Geomech.*, 40(1), 62–79.
- Kafui, K. D., Johnson, S., Thornton, C., and Seville, J. P. K. (2011). "Parallelization of a Lagrangian-Eulerian DEM/CFD code for application to fluidized beds." *Powder Technol.*, 207(1–3), 270–278.
- Kafui, K. D., Thornton, C., and Adams, M. J. (2002). "Discrete particle-continuum fluid modelling of gas–solid fluidized beds." *Chem. Eng. Sci.*, 57(13), 2395–2410.
- Latham, J. P., et al. (2008). "Modelling of massive particulates for break-water engineering using coupled FEMDEM and CFD." *Particuology*, 6(6), 572–583.
- Mori, H., Ogawa, Y., and Cao, G. (2002). "Liquefaction analysis of river dike with discrete element method." *Proc., 3rd Int. Conf. on Discrete Element Methods*, ASCE, Reston, VA, 172–177.
- Nakasa, H., Takeda, T., and Ishikawa, H. (1999). "A liquefaction analysis aim to investigation of behavior of to the ground surrounding the nuclear power plant during or after strong earth quakes (a simulation study on liquefaction using DEM)." *Proc., 7th Int. Conf. on Nuclear Engineering*, ASME, New York, 1–9.
- Nicot, F., Hadda, N., Guessasma, M., Fortin, J., and Millet, O. (2013). "On the definition of the stress tensor in granular media." *Int. J. Solid Struct.*, 50(14–15), 2508–2517.
- Pain, C. C., et al. (2005). "Three-dimensional unstructured mesh ocean modelling." *Ocean Modell.*, 10(1–2), 5–33.
- Pain, C. C., Umpheby, A. P., de Oliveira, C. R. E., and Goddard, A. J. H. (2001). "Tetrahedral mesh optimisation and adaptively for steady-state and transient finite element calculation." *Comput. Methods Appl. Mech. Eng.*, 190(29–30), 3771–3796.
- PFC<sup>3D</sup> 4.0* [Computer software]. Itasca Consulting Group, Minneapolis.
- Potyondy, D. O., and Cundall, P. A. (2004). "A bonded-particle model for rock." *Int. J. Rock Mech. Min. Sci.*, 41(8), 1329–1364.
- Risnes, R., Bratli, R. K., and Horsrud, P. (1982). "Sand stresses around a wellbore." *Soc. Pet. Eng. J.*, 22(6), 883–898.
- Takada, S., and Hayakawa, H. (2016). "Drag law of two-dimensional granular fluids." *J. Eng. Mech.*, 10.1061/(ASCE)EM.1943-7889.0001054, C4016004.
- Tsuji, Y., Kawaguchi, T., and Tanaka, T. (1993). "Discrete particle simulation of two-dimensional fluidized bed." *Powder Technol.*, 77(1), 79–87.
- Viré, A., et al. (2012). "Modelling of fluid–solid interactions using an adaptive mesh fluid model coupled with a combined finite–discrete element model." *Ocean Dyn.*, 62(10), 1487–1501.